AD-A097 040 PURDUE UNIV LAFAYETTE IND SCHOOL OF MECHANICAL ENGI--ETC F/G 14/2
INVESTIGATION OF BIAS ERRORS IN LASER DOPPLER VELOCIMETER MEASU--ETC(U)
DEC 80 T C ROESLER, W H STEVENSON F33615-77-C-2010

UNCLASSIFIED AFWAL-TR-80-2105 NL

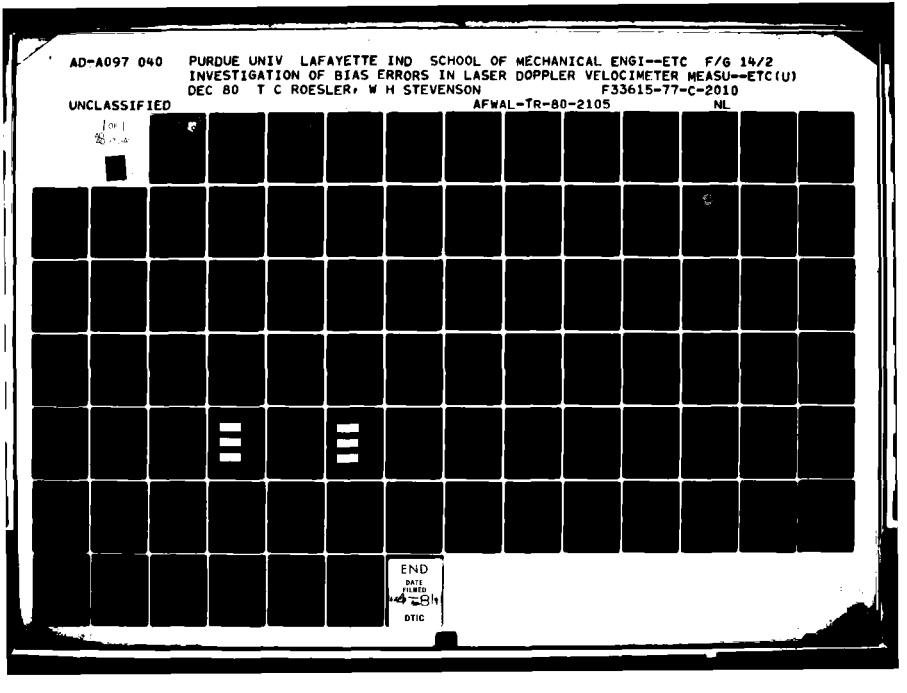

AFWAL-TR-80-2105

LEVEL II

2

P) 5

AD A09

INVESTIGATION OF BIAS ERRORS IN LASER DOPPLER VELOCIMETER MEASUREMENTS

TIMOTHY C. ROESLER
W.H. STEVENSON
H. DOYLE THOMPSON

SCHOOL OF MECHANICAL ENGINEERING
PURDUE UNIVERSITY
WEST LAFAYETTE, INDIANA 47907

DECEMBER 1980

TECHNICAL REPORT AFWAL-TR-80-2105
Interim Technical report for period June 1978 - July 1980

Approved for public release; distribution unlimited.

AERO PROPULSION LABORATORY
AIR FORCE WRIGHT AERONAUTICAL LABORATORIES
AIR FORCE SYSTEMS COMMAND
WRIGHT-PATTERSON AIR FORCE BASE, OHIO 45433

NOTICE

When Government drawings, specifications, or other data are used for any purpose other than in connection with a definitely related Government procurement operation, the United States Government thereby incurs no responsibility nor any obligation whatsoever; and the fact that the government may have formulated, furnished, or in any way supplied the said drawings, specifications, or other data, is not to be regarded by implication or otherwise as in any manner licensing the holder or any other person or corporation, or conveying any rights or permission to manufacture, use, or sell any patented invention that may in any way be related thereto.

This report has been reviewed by the Office of Public Affairs (ASD/PA) and is releasable to the National Technical Information Service (NTIS). At NTIS, it will be available to the general public, including foreign nations.

This technical report has been reviewed and is approved for publication.

Roger R. Craig
Project Engineer

Frank D. Stull, Chief
Ramjet Technology Branch
Ramjet Engine Division

FOR THE COMMANDER

Edward T. Curran

E.T. Curran, Deputy Director
Ramjet Engine Division

"If your address has changed, if you wish to be removed from our mailing list, or if the addressee is no longer employed by your organization please notify AFWAL/PORT Attn: Roger Craig W-PAFB, OH 45433 to help us maintain a current mailing list".

Copies of this report should not be returned unless return is required by security considerations, contractual obligations, or notice on a specific document.

AIR FORCE/56780/10 March 1981 —100

SECURITY CLASSIFICATION OF THIS PAGE (When Data Entered)

REPORT DOCUMENTATION PAGE

READ INSTRUCTIONS BEFORE COMPLETING FORM

1. REPORT NUMBER: AFWAL-TR-80-2105	2. GOVT ACCESSION NO.: AD-A097040
3. RECIPIENT'S CATALOG NUMBER:	
4. TITLE (and Subtitle): Investigation of Bias Errors in Laser Doppler Velocimeter Measurements	5. TYPE OF REPORT & PERIOD COVERED: Interim Technical Report, Jun 78 - Jul 80
	6. PERFORMING ORG. REPORT NUMBER:
7. AUTHOR(s): Timothy C. Roesler, C.H. Stevenson and H. Doyle Thompson	8. CONTRACT OR GRANT NUMBER(s): F33615-77-C-2010
9. PERFORMING ORGANIZATION NAME AND ADDRESS: School of Mechanical Engineering, Purdue University, West Lafayette, IN 47907	10. PROGRAM ELEMENT, PROJECT, TASK AREA & WORK UNIT NUMBERS: 2308-S1-02
11. CONTROLLING OFFICE NAME AND ADDRESS: Aero Propulsion Laboratory (AFWAL/PORT), Air Force Wright Aeronautical Laboratories (AFSC), Wright-Patterson Air Force Base, Ohio 45433	12. REPORT DATE: Dec 80
	13. NUMBER OF PAGES: 78
14. MONITORING AGENCY NAME & ADDRESS (if different from Controlling Office)	15. SECURITY CLASS. (of this report): UNCLASSIFIED
	15a. DECLASSIFICATION/DOWNGRADING SCHEDULE

16. DISTRIBUTION STATEMENT (of this Report)

Approved for public release; distribution unlimited.

17. DISTRIBUTION STATEMENT (of the abstract entered in Block 20, if different from Report)

18. SUPPLEMENTARY NOTES

19. KEY WORDS (Continue on reverse side if necessary and identify by block number)

Turbulence measurements
Laser velocimeter
Bias errors (in laser velocimetry)

20. ABSTRACT (Continue on reverse side if necessary and identify by block number)

The problem of velocity bias in laser Doppler Velocimeter (LDV) measurements made with counter type (burst) signal processors in turbulent flows was investigated. By using a signal processing technique which allowed velocity samples to be taken either randomly or at equal time intervals, the magnitude of the velocity bias was directly measured under various flow conditions. Using this technique, the validity of the one-dimensional velocity weighting correction of McLaughlin and Tiederman was investigated and found to be useful

DD FORM 1 JAN 73 1473 EDITION OF 1 NOV 65 IS OBSOLETE
S/N 0102-014-6601

SECURITY CLASSIFICATION OF THIS PAGE (When Data Entered)

only at turbulence intensities below about 20 percent.

Incomplete signal bias was also investigated and found to cause serious errors in unshifted LDV measurements. However, this bias may be virtually eliminated by frequency shifting.

PREFACE

This interim report was submitted by the School of Mechanical Engineering of Purdue University, under Contract No. F33615-77-C-2010 and covers the period 1 June 1978 - 31 July 1980. The effort was sponsored by the Aero Propulsion Laboratory, Air Force Wright Aeronautical Laboratories, Wright-Patterson AFB, Ohio under Project No. 2308 with Roger R. Craig/AFWAL/PORT as Project Engineer. Warren H. Stevenson and H. Doyle Thompson of Purdue University were technically responsible for the work.

TABLE OF CONTENTS

LIST OF ILLUSTRATIONS

LIST OF TABLES

NOMENCLATURE

A_p	Cross-sectional area of probe volume
D_m	Digital mantissa of TSI processor
D_p	Diameter of probe volume
E_T	Analog output of TSI processor
F_r	Fringe Spacing
f_D	Doppler frequency
f_s	Shift frequency
N	Number of cycles/burst
N_T	Total number of fringes in probe volume
n	Exponent on TSI processor
S	Average velocity gradient across probe volume
T_r	Reset time of TSI processor
$\overline{U}$	Mean velocity component
U_i	Individual velocity realization
u'	RMS velocity (standard deviation)
V	Velocity vector
V_F	Fringe velocity
w_o	Radius of Gaussian beam
α	Angle between velocity vector and fringe normal
λ	Laser light wavelength
ω_i	Weighting factor

SECTION I

INTRODUCTION

The laser Doppler velocimeter (LDV) has gained wide acceptance as a measuring instrument in fluid mechanics research, particularly for turbulent flow studies. However, questions have arisen regarding the accuracy of LDV measurements under certain conditions. When a counter type (burst) processor is used for LDV signal processing, for example, it has been suggested that the measured mean velocity may be in error due to a "velocity bias". A number of investigations related to this problem have been conducted in recent years, but the results have not been conclusive.

A primary objective of the present investigation was to develop a method for direct measurement of velocity bias in a turbulent flow and to determine if it could be eliminated by proper signal processing techniques. The validity of one of the more common velocity bias correction schemes was also studied. In addition a second important bias error, incomplete signal bias, was investigated.

Results of the investigation show that velocity bias does exist and can cause significant errors in turbulent flow measurements. However, it can be eliminated by proper signal processing techniques. The magnitude of the bias is strongly dependent upon the manner in which data is taken and the flow structure. Therefore, correction schemes which do not take these factors into account are inadequate

and may, in fact, increase the error. Incomplete signal bias was also found to be significant, but it can be minimized by frequency shifting as previous studies have shown.

SECTION II

LITERATURE REVIEW

1. Introduction

Turbulent flow is by definition fluctuating, random, and three dimensional. As a result, measurements in turbulent flows are difficult to perform. Hinze [1] suggests six requirements which an instrument must meet to make accurate turbulent measurements:

1. The probe must cause minimal disturbance to the flow.
2. The probe must be smaller than the smallest turbulent structure.
3. The instrument must have a fast response time.
4. The instrument must be sensitive enough to record small velocity changes.
5. The calibration of the instrument must not change over the time required to make a series of measurements.
6. The probe must be strong enough to withstand the forces exerted by the flow.

The laser Doppler velocimeter (LDV) is unique among flow measurement instruments because it is capable of meeting all six of Hinze's requirements.

Since 1968 the LDV has undergone a great deal of development, much of which has been reported in various symposium proceedings [2,3,4,5]. As a result of this work, several sources of error have been discovered which are inherent in LDV measurements. Many of these

errors have been fully analyzed and are easily eliminated or reduced to an insignificant level. However, velocity bias continues to be a problem in turbulent flow measurements. Several correction schemes designed to reduce velocity bias errors have been developed, but their effectiveness is not known. Incomplete signal bias can also be a problem in some cases. Recent literature dealing with velocity bias, incomplete signal bias and other errors will be reviewed in the following sections.

2. Velocity Bias

The existence of a velocity bias in data obtained with counter type processors was first proposed by McLaughlin and Tiederman [6] in 1973. They suggested that the probability of a velocity realization is dependent on the velocity as shown by

$$\Delta n = |V| A_p M \Delta t \qquad (1)$$

where Δn is the average number of velocity realizations obtained during any time interval, Δt is the length of the time interval, $|V|$ is the magnitude of the velocity vector, A_p is the projected area of the probe volume normal to V, and M is the seed density.

As a result, the mean velocity obtained from an ensemble average of LDV data points in a steady turbulent flow will be biased to higher values. They suggested correcting for the bias by weighting each velocity realization by the inverse of the magnitude of the velocity vector. For a spherical probe volume, the mean velocity $\overline{U}$ and RMS velocity u' would then be given by

$$\bar{U} = \frac{\sum_{i=1}^{M} \frac{1}{|V_i|} U_i}{\sum_{i=1}^{M} \frac{1}{|V_i|}} \tag{2}$$

$$u' = \left[\frac{\sum_{i=1}^{M} \frac{1}{|V_i|} (U_i - \bar{U})^2}{\sum_{i=1}^{M} \frac{1}{|V_i|}} \right]^{1/2} \tag{3}$$

where $\bar{U}$ is the mean velocity, U_i is an individual velocity realization, $|V_i|$ is the magnitude of the instantaneous velocity vector, and u' is the RMS velocity.

Generally, the magnitude of the velocity vector is not known. McLaughlin and Tiederman suggested that at lower turbulence levels the magnitude of the instantaneous velocity vector is approximately the same as the magnitude of the velocity component being measured. However, in flows where there is a high probability of having large velocity components perpendicular to the fringes, this one-dimensional correction tends to over correct the mean velocity.

George [7] arrived at a correction for the mean velocity by weighting each velocity realization by a particle's residence time in the probe volume and then expressing that time as a function of velocity and probe volume size.

Buchave [8] pointed out that the overcorrection produced by the one-dimensional weighting at high turbulence levels is partially compensated for because of the N-fringe requirement of most counters which introduces incomplete signal bias. He concluded that if the

one-dimensional correction is used along with frequency shift, the measurement error may actually be increased in some cases due to the elimination of this compensating effect.

Barnett and Bentley [9] analyzed velocity bias using a series representation of the time average velocity

$$\overline{U} = \frac{1}{T} \sum_{i=1}^{M} U_i \, \Delta t_i \tag{4}$$

where Δt_i is the time between samples and T is the total sampling interval. They assumed that in uniformly seeded flows the time between samples is correlated with the average velocity over the interval. They concluded, as did McLaughlin and Tiederman, that a true time average could be obtained by weighting each velocity realization by the inverse of velocity. However, Barnett and Bentley also concluded that if the particles are separated by long times the correlation between velocity and time is destroyed. Thus if the particle arrival rate is much lower than the frequency of velocity oscillations, velocity bias will not exist. This result is in direct conflict with McLaughlin and Tiederman's conclusion [6] that bias will exist regardless of the particle arrival rate.

Hoesel and Rodi [10] observed that the one-dimensional correction of McLaughlin and Tiederman was too restrictive because it required uniform seeding. They proposed two different corrections. In uniformly seeded flows, they suggested weighting each velocity realization by the particle's residence time in the probe volume.

The particle's residence time may be calculated from its mean velocity and from the total number of fringes it crosses in the probe

volume. Processors which determine the total number of fringe crossings are now commercially available. In non-uniformly seeded flows, they suggested weighting by the time between bursts. However, the time must be measured from one burst to the next regardless of whether or not this second burst has sufficient amplitude to be detected which presents a practical difficulty. Hoesel and Rodi presented experimental data taken in a free jet. However, no attempt was made to compare their results with independent measurements so no definite conclusion concerning the validity of their correction scheme can be made.

Kreid [11] showed that velocity gradients in the probe volume may cause bias similar to that cited by McLaughlin and Tiederman. He concluded that a linear velocity gradient would cause a positive bias (increased measured mean velocity) while second order gradients may cause either positive or negative bias. However, Kreid concluded that, in most instances, the effects of gradients are negligible.

Karpuk and Tiederman [12] performed an analysis similar to that of Kreid except they considered the effects of velocity gradients and turbulence on both the mean and RMS velocities. The analysis showed that the one-dimensional velocity weighting is applicable when calculating mean velocities in turbulent flows with velocity gradients. Velocity profiles from the viscous sublayer of a water channel were calculated from pressure gradient measurements and compared to profiles obtained with an LDV. The uncorrected LDV profiles contained velocities approximately 10% higher than the profiles calculated from the pressure gradient information, while the LDV profiles calculated using the

one-dimensional velocity weighting were significantly closer to the pressure gradient profiles.

Karpuk and Tiederman also analyzed the calculation of the RMS velocity in turbulent flows with a velocity gradient. Their analysis showed that the total variance comes from three sources, namely turbulence, the mean velocity gradient, and the gradient of the variance. It was also shown that the one-dimensional velocity weighting does not account for the two spatial (gradient) effects. They suggested the following correction

$$u_o'^2 = \frac{u_m'^2 - \frac{S^2 D_p^2}{12}}{1 + \frac{S^2 D_p^2}{12 U_o^2}} \qquad (5)$$

where u_o' is the "true" RMS velocity at the center of the probe volume, u_m' is the RMS velocity calculated using the one-dimensional velocity weighting, U_o is the mean velocity at the center of the probe volume (calculated using one-dimensional velocity weighting), D_p is the width of the probe volume and S is the average velocity gradient across the probe volume. LDV data taken outside of the viscous sublayer was compared with similar hot film data taken by Eckelmann and Reichardt [13]. The uncorrected and one-dimensional velocity weighted standard deviations were significantly higher than the hot film results. However, their proposed correction yielded good agreement with the hot film data.

Meyers and Clemmons [14] noted that if a high sampling rate is used, it is possible to obtain multiple samples from a single particle.

This is especially true in LDVs which use frequency shifting. Multiple sampling results in velocities being biased to lower values because slower particles spend more time in the probe volume and are more likely to be sampled several times. Meyers and Clemmons termed this effect Bragg bias and claim that it partially compensates for velocity bias. They suggest correcting LDV data by weighting each realization by the inverse of the product of the velocity and the number of possible realizations from each particle. The resultant weighting factor is given by

$$\omega_i = \frac{N F_r + T_r(V_F + U_i)}{D_p(V_F + U_i)} \tag{6}$$

where N is the number of fringes required for a realization, F_r is the fringe spacing, T_r is the reset time of the processor, V_F is the fringe velocity, U_i the particle velocity, and D_p is the diameter of the probe volume. However, this factor does not take into account the fact that the number of realizations from a particle must be an integer, so it is obviously incorrect.

Durao and Whitelaw [15] suggested using random sampling to reduce velocity bias, since using all of the velocity realizations tends to maximize bias error. Random sampling of the data should lessen the effects of many closely spaced signals. They presented artificial data created by randomly sampling a sine wave which showed that random sampling does reduce the measured mean velocity. However, their results for actual Doppler signals were much less conclusive. In any case, the reduction in the mean velocities observed may not have been

the direct result of random sampling but rather due to sampling at more equal times as the average interval between samples increased.

In a later paper Durao and Whitelaw [16] experimentally found a variation in Doppler frequency with particle arrival time. They suggested weighting velocity realizations by their arrival time. However, no mention of how the arrival time of a particle is defined or how it was determined was mentioned.

Giel and Barnett [17] performed LDV measurements in a free jet and compared the results to hotwire measurements. They found no evidence of velocity bias, but suggested using a heavily seeded flow sampled at a very slow rate as a means of avoiding biased results.

Bogard and Tiederman [18] investigated the effect of particle arrival rate and particle velocity on velocity bias. They found that neither had any effect on velocity bias.

Buchave [19] has recently completed an extensive analytical and experimental study of biasing. He concludes that a residence time weighting provides the correct statistical results in uniformly seeded flows, since it is equivalent to a time averaging of the data. His experiments included measurements in a free jet using a hot wire and a frequency shifted LDA with both tracker and counter type processors. It was assumed that the LDA tracker gave the "true" mean velocity. Based on this assumption the residence time weighting provided the proper bias correction over a wide range of turbulence intensity. The M-T one-dimensional correction, on the other hand, significantly over-corrected the counter data once the turbulence intensity exceeded 10-20 percent. This is to be expected, since the M-T correction is known to be invalid at high turbulence levels. It should be noted that Buchave

found an 8% difference between the hotwire and tracker results on the jet axis with even larger differences off-axis.

Table 1. Proposed Velocity Bias Corrections.

$$\overline{U} = \sum_{i=1}^{M} \omega_i U_i / \sum_{i=1}^{M} \omega_i$$

ω_i	Suggested by	Description
$\frac{1}{\lvert V_i \rvert}$	McLaughlin & Tiederman	weight by the inverse of the magnitude of the velocity vector (Requires measurement of total vector.)
$\frac{1}{\lvert U_i \rvert}$	McLaughlin & Tiederman	weight by the inverse of the magnitude of the measured component (Simplified 1-D correction.)
t_p	George	weight by the particle's residence time in the probe volume
t_i	Hoesel & Rodi	weight by time between particles
$\frac{1}{\lvert U_i \rvert n_i}$	Meyers & Clemmons	weight by inverse of the product of the measured velocity component and the maximum number of realizations from a particle

A summary of the schemes discussed is presented in Table 1. It is apparent from the literature reviewed here that the velocity bias question is still open. The "proper" correction method to be used is not clear and there have in fact been no definitive experiments which conclusively demonstrate the existence of velocity bias. A primary problem has been the difficulty of obtaining accurate unbiased measurements in a turbulent flow.

3. Incomplete Signal Bias

When counter type processors are operated in the N cycle mode (N Doppler cycles required to acquire a valid output) incomplete signal bias may exist in a turbulent flow. A particle crossing the LDV probe volume at an angle to the fringe normal may not cross enough fringes to produce the required N cycles and therefore this velocity data is lost. Generally, such particles would have a velocity component normal to the fringes which is lower than the mean velocity. Their failure to be counted results in the ensemble averaged mean velocity being biased to a higher value. It has been pointed out that LDVs without frequency shifting may therefore not have the required isotropic response to make accurate measurements in highly turbulent flows. Frequency shifting reduces incomplete signal bias by increasing the number of fringes seen by a particle crossing the probe volume. Whiffen, Lau, and Smith [20] derived an expression for the "polar response" of a probe volume as a function of the effective cross sectional area.

The effective cross section of the probe volume is defined as the area of the circle with diameter equal to the width of the region through which a particle traveling at a given angle must pass in order to cross the required number of fringes. This is illustrated in Figure 1. The polar response is this effective area nondimensionalized by dividing by the actual area of the probe volume. The polar response is given as a function of the particle's incidence angle by:

$$PPD(\alpha) = \left[1 - \left(\frac{N/N_T}{\cos\alpha + V_F/|V|} \right)^2 \right]^{1/2} \qquad (7)$$

where N is the required number of fringe crossings, N_T is the total number of fringes in the probe volume, α is the angle of incidence of the particle, V_F is the fringe velocity (assumed positive if the fringes move opposite the flow direction), and $|V|$ is the magnitude of the velocity vector.

A plot of the polar response of a probe volume is shown in Figure 2 for $N/N_T = 0.75$ and various values of $V_F/|V|$. Note that when no frequency shift is used ($V_F/|V| = 0$) the probability that a particle entering the probe volume perpendicular to the fringes will cross the required number of fringes is less than 0.75 and the probability of detection decreases to zero at entrance angles greater than ±60°. However, when $V_F/|V| = 2$ (fringes are moving at two times the particle velocity but in the opposite direction), particles entering the probe volume at any angle have a probability greater than 0.7 of crossing N fringes while particles entering at angles between ±90° (90° is parallel to the fringes) have a probability greater than 0.9 of crossing N fringes. Thus, incomplete signal bias may be significantly reduced by frequency shifting.

4. Other Measurement Errors

Thompson and Flack [21] described ten bias errors which may occur in LDV measurements. Two of these are velocity bias and incomplete signal bias as were described in the previous sections. The remaining

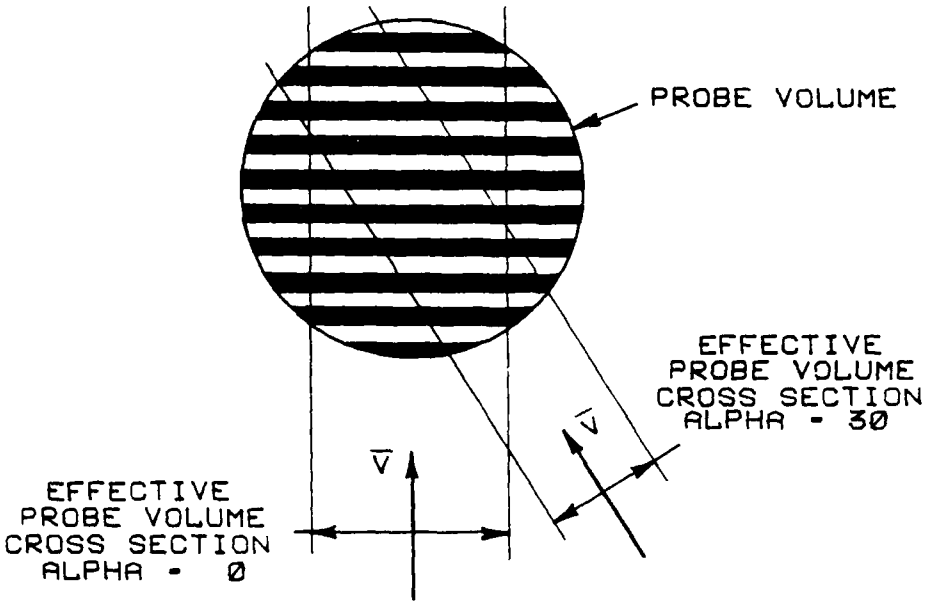

Figure 1. Effective probe volume cross section.

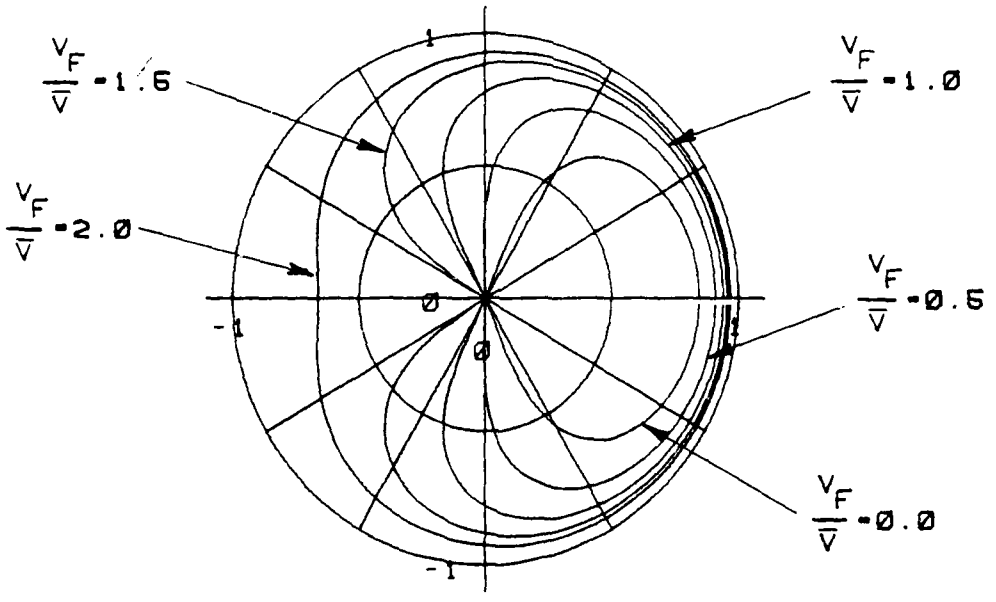

Figure 2. Polar response of a probe volume.

biases are generally considered to be well understood and can be minimized with proper equipment and signal processing. However, if they are ignored, serious errors may result. These biases and other error sources will be briefly examined here.

Frequency broadening may result if the two beams of the LDV do not cross at their beam waists. Hanson [22] and Durst and Stevenson [23] have investigated this problem and have shown that with a properly designed and aligned system, frequency broadening may be eliminated.

Directional ambiguity results from the LDV's inability to distinguish between plus and minus velocities. Generally, it is only a problem in regions containing reverse flows, although it can also affect measurements made in regions of high turbulence. Durst and Zaré [24] suggested several methods of eliminating directional ambiguity, the most common being frequency shifting.

Counters which use a high speed digital clock may have clock errors from two sources. The first is the result of the finite period of a clock cycle. The second results from the lack of synchronization of the gating of the clock with the beginning and end of the Doppler burst. Wang [25] investigated this problem and showed that, in some cases, the period measurement will always be zero to one clock cycle too many. However, with the development of higher clock speeds such clock errors have become less significant.

Particle distribution bias results from non-uniform seed distribution in the flow. Non-uniform seed distributions often occur in mixing or reacting flows. Giel and Barnett [17] and Asalor and Whitelaw [26] have examined this problem, but the results are

conflicting. More work needs to be done in this area.

Particle lag bias is the result of large particles not accurately following the flow fluctuations. However, in many situations, seed size is easily controlled. Also, processors are now being produced with circuitry which eliminates high amplitude signals resulting from large particles.

Most counters require the Gaussian pedestal to be removed from the Doppler signal before processing. Generally, this is performed electronically with a high pass filter. However, filtering is only effective if the spectral band width of the pedestal does not overlap the Doppler spectrum. Should overlap occur, it may be eliminated by frequency shifting or the pedestal may be removed optically [24].

Two related biases are comparator tolerance bias and particle acceleration bias. Most counters validate signals by comparing the measured times for different numbers of Doppler cycles (4/8, 16/32, etc.). Should the tolerance on this comparison be set too low, signals from particles which accelerate through the probe volume will be eliminated. Thompson and Flack [21] recommend a tolerance setting of no less than 5% for turbulent flow measurements.

SECTION III

SYSTEM DESIGN

1. Introduction

The LDV system used in this investigation was designed specifically for studying bias errors. Its flexible design allows for variation of several optical parameters as well as various data and sampling rates. The system may be divided into four subsystems:

1) The LDV
2) The flow system
3) The data acquisition system
4) The seeding system.

2. LDV Design

The LDV system was designed specifically for studying various bias errors. It has provisions for changing the probe volume size, the fringe spacing, and the angular orientation of the probe volume. It is also possible to frequency shift the beams with a dual Bragg cell system. The general layout of the device is shown in Figure 3. The flexibility of this system allows the probe volume characteristics to be varied over a wide range. However, it also requires a rather careful alignment to insure that the desired conditions are obtained.

Laser light for the system is supplied by a 5 watt Argon laser. The beam exits the laser and enters a polarization rotator. The polarization rotator insures maximum fringe contrast in the probe volume. Following the polarization rotator is the beam expander telescope. The

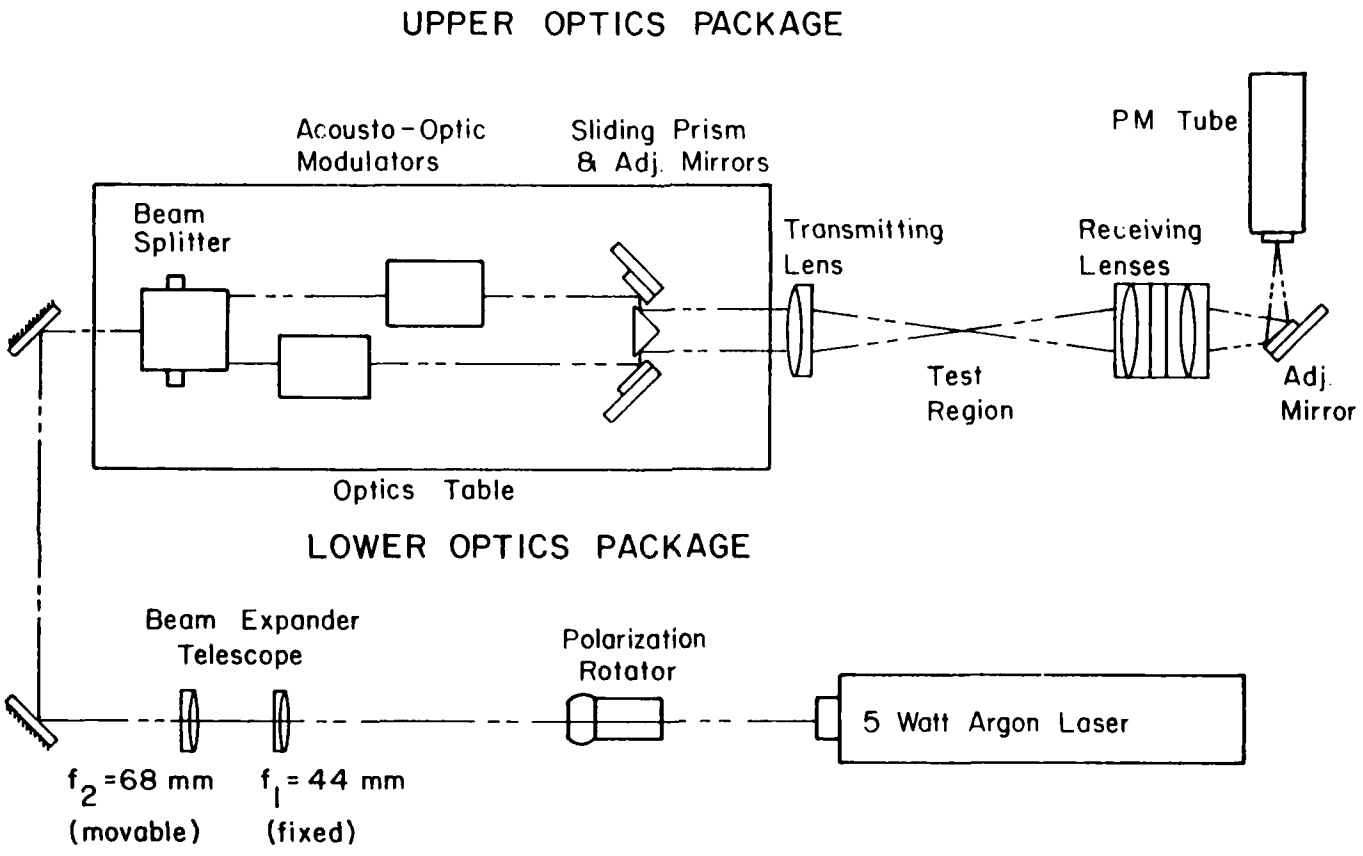

Figure 3. LDV system.

telescope is composed of a 44 mm lens (f_1) followed by a 68 mm lens (f_2). The f_1 lens images the beam waist from inside the laser cavity to a point between the two telescope lenses. Then lens f_2 and the transmitting lens image this waist to a location within the test region. Waist diameters of 60 to 500 μm can be obtained within the test region by moving f_2 over a 7.5 mm traverse.

From the telescope, the beam is reflected to the upper portion of the transmitting optics package where it enters the beam splitter. The beam splitter is a commercial TSI model #916-1 which splits the entering beam into two parallel equal intensity beams separated by 50 mm.

Following the beam splitter are the two acousto-optic modulators. The modulators shift the frequency of the incoming beam either up or down by an amount equal to the frequency of the driver. Drivers of 30 and either 35 or 40 MHz are used. (Selection of a 35 or 40 MHz shift involves changing the crystal oscillator in the driver.) By using various combinations to shift one or both beams, net frequency upshifts or downshifts of 0, 5, 10, 30, 35, 40, 70, or 75 MHz are available. A positive frequency shift is defined here as a shift which causes the fringes to move opposite the direction of the fluid flow (increases effective Doppler frequency). Conversely, with a negative shift the fringes move the same direction as the flow and the effective Doppler frequency is decreased.

Next the beams are reflected by the adjustable mirrors to the sliding prism. The prism directs the beams to the transmitting lens. Various beam separations can be obtained by translating the prism. The adjustable mirrors are used to position the beams so that they cross

on the optical axis and at the beam waist. Thus fringe spacing may be changed through proper adjustment of the sliding prism and adjustable mirrors. The transmitting lens has a focal length of 250 mm.

The receiving lenses are a 250 mm lens, similar to the transmitting lens, and a 120 mm lens mounted several centimeters apart. The receiving lenses and the entire receiving optics package may be moved along the axis of the optical system to allow proper focusing.

The optics table is mounted in bearings which rotate on the optical axis. Rotation of the optics table rotates the probe volume so that velocity components at various angles to the horizontal can be measured. A detailed description of the entire system is given by McVey [27].

3. Flow System

The flow system was designed to provide flows with both low and high turbulence intensity while providing easy optical access. The general layout of the system is shown in Figure 4. Its major elements are:

1. A variable speed blower
2. A flow conditioning section
3. The test section
4. An exhaust system
5. The seeding system

The blower is a Peerless Model PWB14GA radial blade blower driven by a variable speed direct current motor. The blower-motor combination is capable of producing air velocities up to 50 m/s at the centerline of the flow conditioner duct downstream of the flow straighteners.

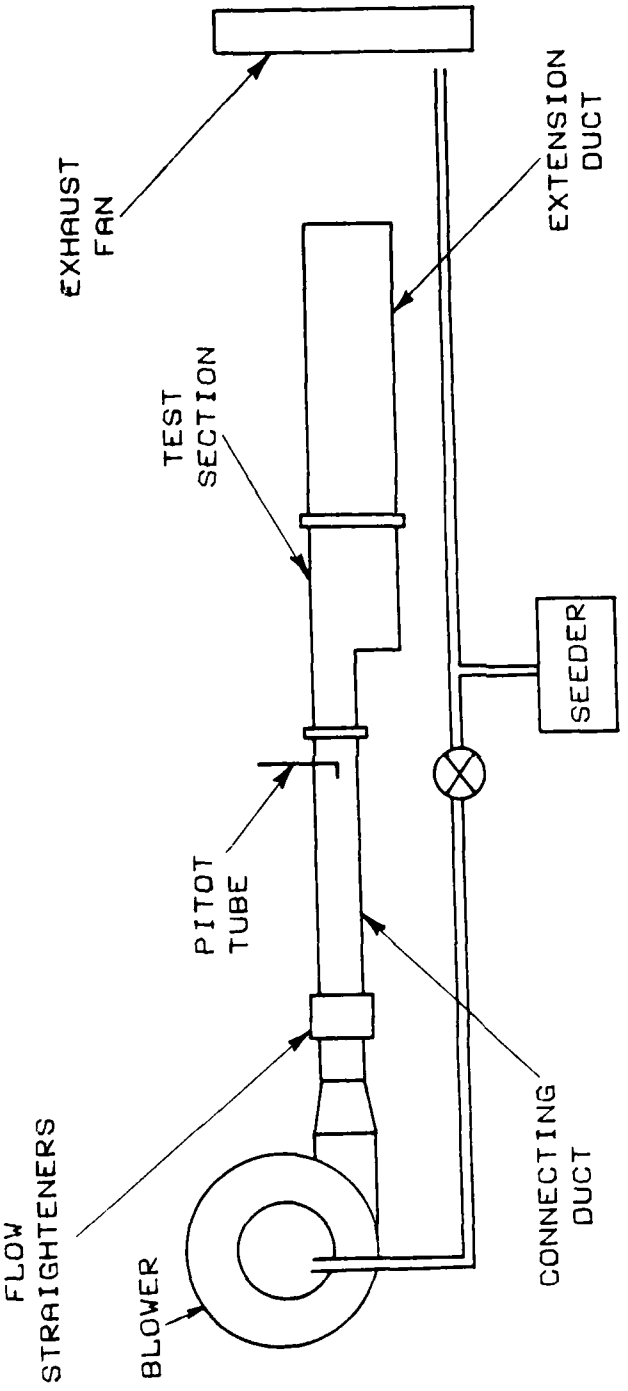

Figure 4. Flow system.

The blower requires approximately one hour of running before its speed stabilizes. After an hour the blower speed continues to fluctuate, but the changes are very small. Generally blower speed is checked prior to each run by a pitot tube located at the centerline of the flow conditioning duct and minor corrections made if necessary. The blower is attached to a separate stand with rubber mounts to eliminate vibrations.

The flow conditioning section consists of a set of flow straighteners followed by a 102 mm by 102 mm (4 in. x 4 in.) duct 1.9 m (24") long. The duct is constructed of 1/2 inch plexiglass. The elements in the flow straightener are an ordinary window screen followed by a honeycomb of 1/4" soda straws one inch long. Following the honeycomb are two more screens. The flow conditioner is attached to the blower through a short duct which is connected to the blower with several wraps of tape. The conditioner and other parts of the flow tube are supported by concrete pillars with provisions for height and level adjustments.

The test section consists of a 102 mm by 102 mm (4 in. x 4 in.) duct which expands into a 102 mm by 204 mm (4 in. x 8 in.) duct over a rearward facing step as shown in Figure 5. It also contains several ports which allow installation of pitot tubes or hot wires. Static pressure taps are located along the top and bottom surfaces of the section as well as along the face of the step. The test section contains flanges at each end which bolt to the flow conditioning duct and a 1.85 m (4.7 in.) extension duct. An exhaust fan is located approximately one meter beyond the exit of the extension duct to

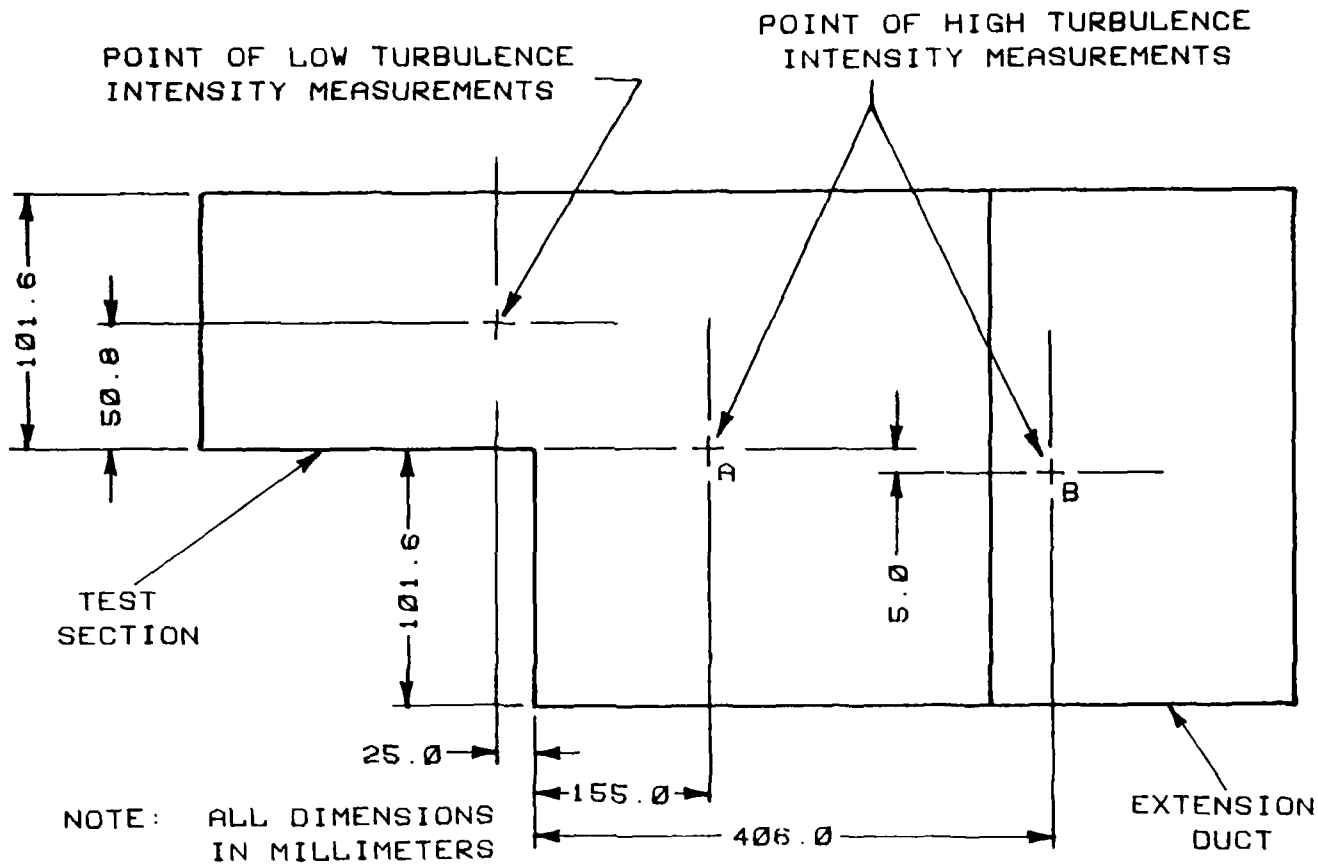

Figure 5. Test section.

remove particle laden air from the room. Most measurements were performed in the shear layer that develops downstream of the step.

The seeder is a commercial system built by TSI. It consists of a Model 3074 air supply, a Model 3076 liquid atomizer, and a Model 3072 Evaporation Condensation Monodisperse Aerosol Generator. Output from the seeder flows through a one gallon bottle, used to damp out flow fluctuations, to a tee. One line from the tee runs to the exhaust fan. The other line runs through a valve to the blower inlet. The seeder may be operated at a constant pressure while the seed density in the flow tunnel is varied by adjusting the valve. High seed densities may be obtained by fully opening the valve and pinching closed the exhaust line. The system produces particles of approximately 1 micron diameter using a solution of 100% DOP (Dioctylphtalate). Smaller particles may be produced by using various solutions of DOP and alcohol. However, the 1 micron particles proved satisfactory for the present study.

4. Signal Processor

The signal processor used was a commercial Thermo-Systems Incorporated (TSI) 1980 processor. The 1980 is a counter processor with 2 ns clock resolution and both digital and analog output. Signals from the photodector are input to the processor's signal conditioner. The conditioner contains low and high pass filters for removing noise and the Gaussian pedestal from the Doppler signal. It also contains an amplifier which varies the amplitude of the filtered signal. Following the conditioner is a timer module. The timer module may be operated in either an N-burst or a total-burst mode. The N-burst mode determines the Doppler frequency from N cycles where N may be set to 2, 4, 8, 16

or 32 cycles per burst. Signal validation is performed with an N/2 to N cycle comparator with a tolerance adjustable from 1 to 20%. In total or T-burst mode the Doppler frequency is determined from all cycles in a burst which exceed a preset minimum amplitude. The minimum number of cycles per burst to be accepted are set when in T-burst mode. However, the comparator may not be used.

The Doppler frequency of a burst is determined in either mode of processor operation using a high speed digital clock in conjunction with a zero crossing detector and a Schmitt trigger, as shown in Figure 6. The Schmitt trigger produces a square wave from that portion of the signal which exceeds the 40 mv threshold. A zero crossing detector generates a pulse each time a rising signal crosses zero volts and the pulse continues until the signal amplitude crosses the 20 mv hysteresis level. The digital clock is gated on at the first zero crossing after the signal has exceeded the threshold voltage. The number of cycles is determined from the zero crossing pulses. If the processor is in N-burst mode, the clock is gated off after N zero crossings. In T-burst mode, the clock is gated off at the first zero crossing after a cycle fails to exceed the threshold. Upon completion of the signal processing, the processor produces a data ready pulse.

Digital output from the processor is in the form of three binary numbers, a 12 bit mantissa, 6 bits for the number of cycles per burst, and a 4 bit exponent. The three values are used to compute a Doppler frequency by

$$f_D = \frac{N \times 10^9}{D_m \times 2^{(n-2)}} \qquad (8)$$

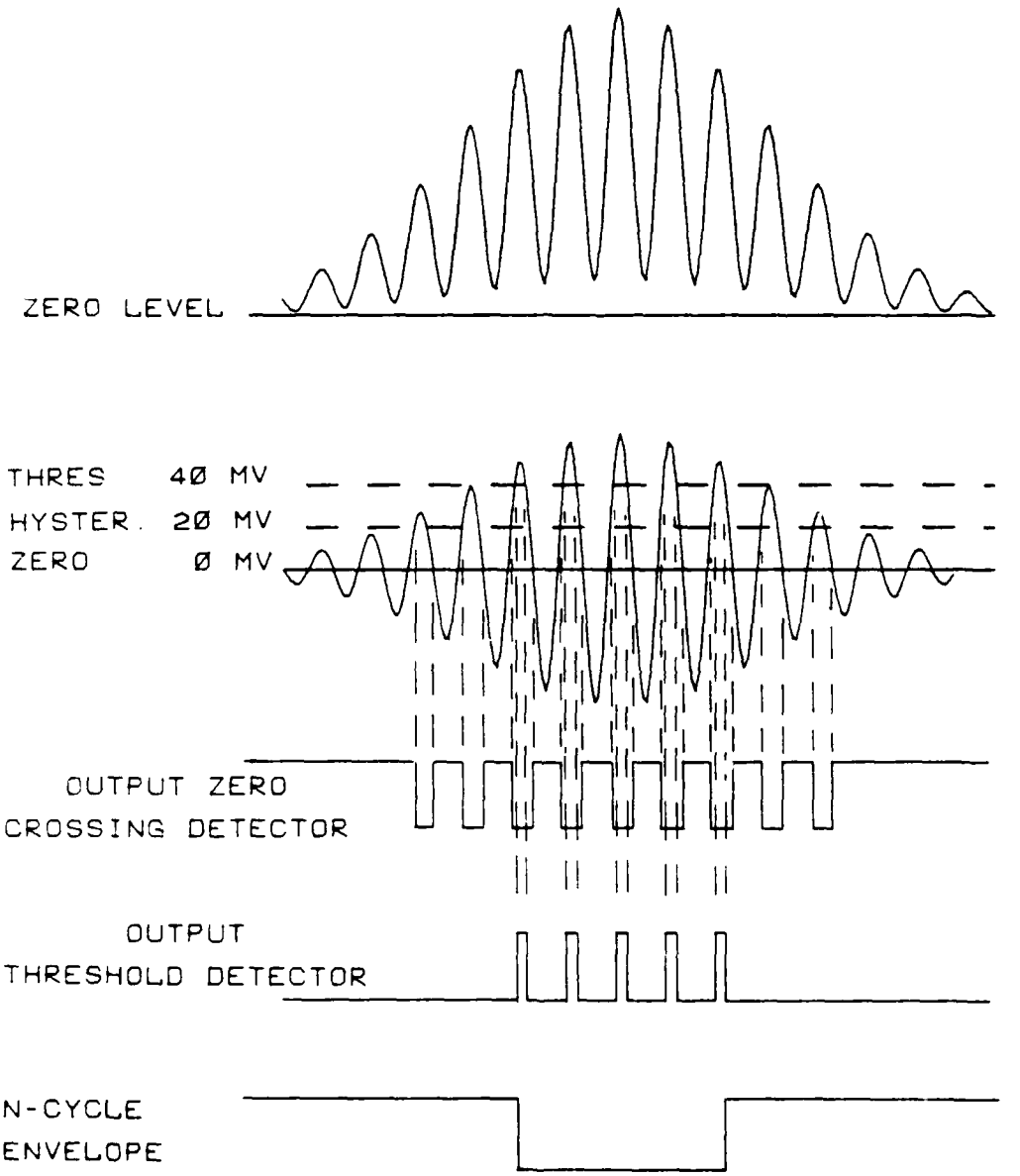

Figure 6. Processor operation.

where N is the cycles per burst, D_m is the digital mantissa, and n is the exponent. If the exponent is set at 3, the mantissa represents the number of 2 ns clock ticks used to measure N cycles. If the exponent is less than 3, one tick of the clock results in a change of $2^{(3-n)}$ in the mantissa. If the exponent is greater than 3, a change in one of the mantissa represents $2^{(n-2)}$ ticks of the clock. The digital output also contains a one bit data ready signal.

Analog output is a 0 to 10 volt signal which varies linearly with velocity. The signal produced by a particle is held until another particle is validated. Therefore, with low seed density and a high sample rate it is possible to obtain more than one sample from a particle. The Doppler frequency may be determined from

$$f_D = \frac{N \times 10^{10}}{E_T \times 2^{(n+10)}} \tag{9}$$

where f_D, N, and n are the same as for the digital output and where E_T is the analog output voltage. The processor contains an output module which displays the average analog voltage and the average data rate.

5. Data Acquisition

Data acquisition and short term data storage are performed by an IMSAI 8080 microcomputer and a Micropolis floppy disk system. Initially, the computer's sampling rate was variable from approximately 0.1 to 2750 samples per second. Recent software modifications have increased the maximum sampling rate to approximately 4800 samples per second. The microcomputer is capable of storing approximately 9500 data points

in memory. After sampling is completed, the data is written on a floppy disk for temporary storage. Each disk is capable of storing approximately 100,000 data points. The microcomputer is also interfaced with the Purdue University Computing Center's CDC 6500 computer. Data may be transfered from floppy disk to the 6500 and permanently stored on magnetic tape. The 6500 is also used for all of the data analysis.

The microcomputer and TSI processor are interfaced such that the microcomputer samples on command of the TSI as shown in Figure 7. When the TSI processor has a data point ready, it sends a data ready pulse to the microcomputer. When the microcomputer receives the pulse, it returns a data inhibit pulse to the TSI processor. The inhibit stops the TSI processor from taking more data and causes it to hold the present data until it can be read. The microcomputer waits a fixed time interval, depending on the desired sampling rate, before reading the data. Once the data is read, the microcomputer removes the data inhibit, stores the data, and waits for another data ready pulse. The rate at which data is recorded is dependent on the slower of the two instruments.

The microcomputer also contains an analog to digital converter for sampling analog signals. Analog signals from 0 to 5 volts are converted to a digital value between 0 and 1024. Analog sampling may be performed at rates up to 4773 Hz.

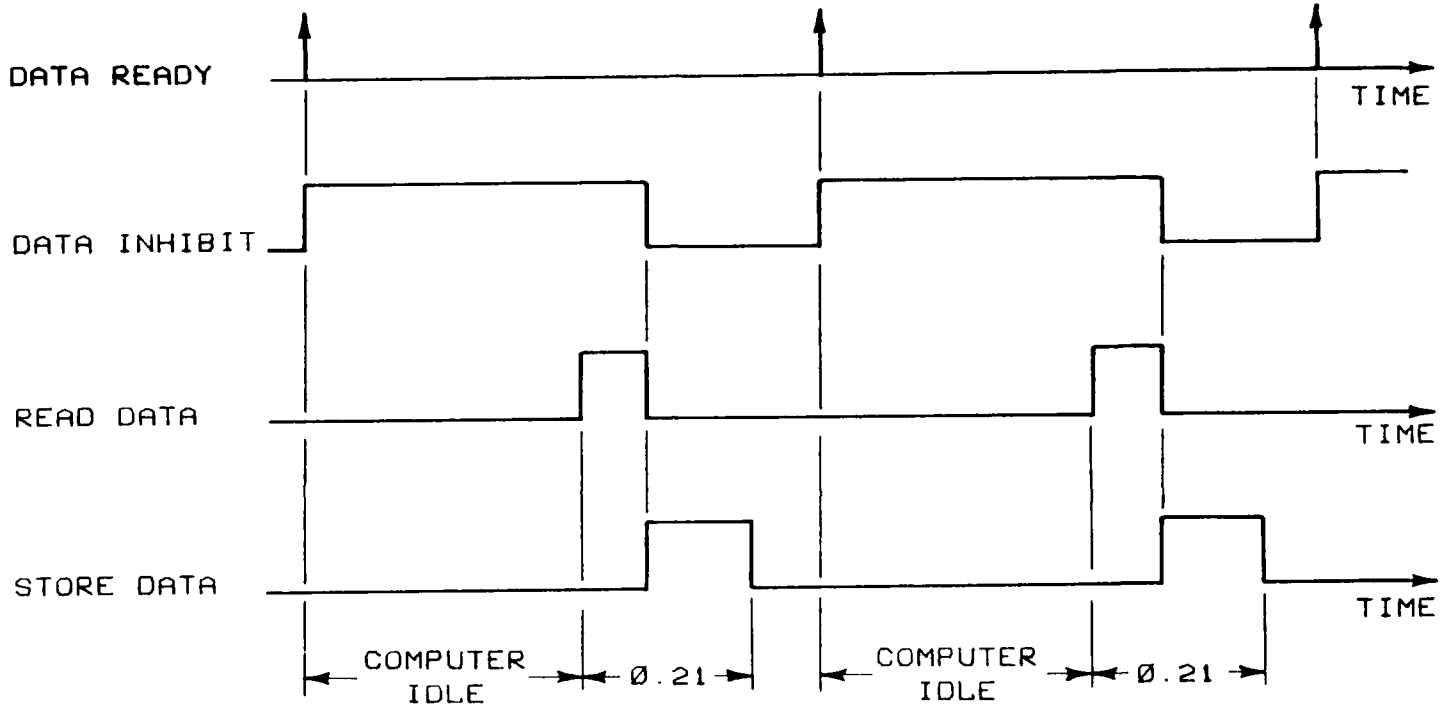

NOTE: TIME IN MILLISECONDS

Figure 7. Microcomputer operation.

SECTION IV

SYSTEM PERFORMANCE

The performance of the TSI processor and LDV were evaluated in two ways prior to making flow measurements. The processor was checked independently of the LDV by sampling 5 and 10 MHz sine waves created by a signal generator. Histograms and the measured mean frequency were determined from the resulting data and compared with those expected. The LDV and TSI processor were evaluated together by sampling photodetector outputs with the TSI processor. The signals were generated by either a glass fiber or a 2.5 μm pin hole fixed in the LDV probe volume. The evaluation was performed using both a 5 and a 10 MHz frequency shift and, as before, histograms and measured mean frequencies were determined and compared with those expected.

Several histograms of the signal generator data are shown in Figures 8, 9, 10, and 11. The spacing between the histogram bars are the result of the processor's finite clock resolution. Each bar represents a difference of one clock cycle.

The histogram in Figure 8 is the result of proper operation of the processor. The majority of the period measurements contain the same number of clock cycles as indicated by the large center bar of the histogram. The shorter bars on either side represent an error of plus or minus one clock cycle in some measurements.

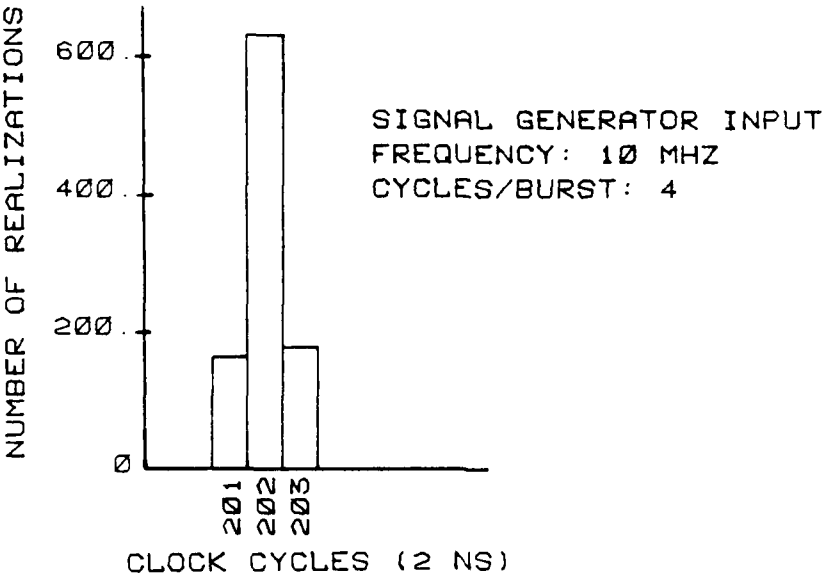

Figure 8. Histogram for 10 MHz signal generator input (N=4).

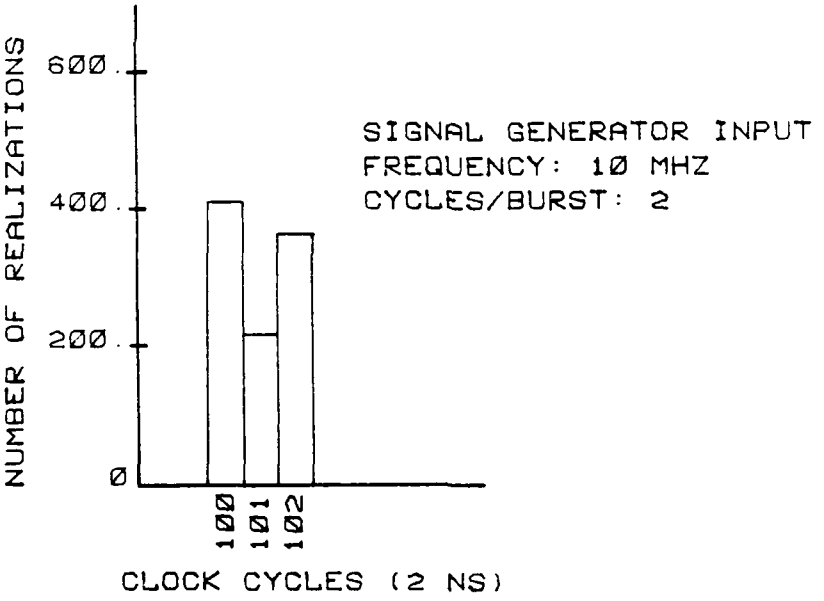

Figure 9. Histogram for 10 MHz signal generator input (N=2).

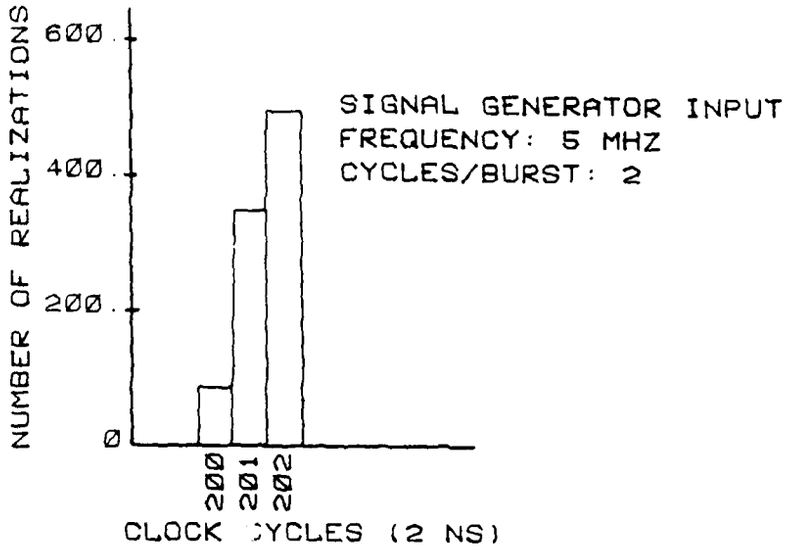

Figure 10. Histogram for 5 MHz signal generator input (N=2).

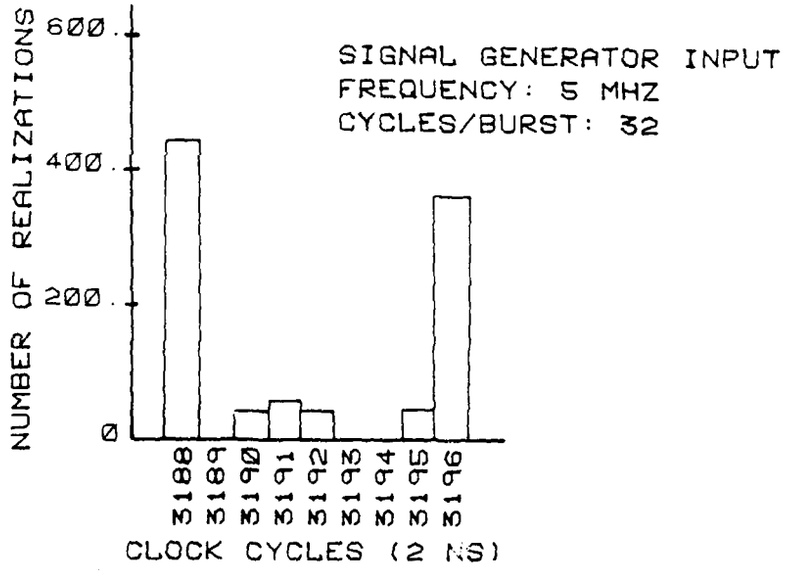

Figure 11. Histogram for 5 MHz signal generator input (N=32).

Typically, the histograms of signal generator data contained three bars. However, very few had the distinct central bar of Figure 8. Many of the histograms contained two major bars separated by a shorter bar as in Figure 9 or one major bar and two smaller bars to one side as in Figure 10. The reason for these differences in the histograms is thought to be the result of the processor having a preference for certain digital values. Occasionally, a histogram similar to Figure 11 was produced. These very wide histograms are probably the result of noise and signal distortion.

Mean quantities of the 5 and 10 MHz signal generator data are shown in Tables 2 and 3. The "velocity" information is based on a 4.339 μm fringe spacing and a shift frequency equal to the input frequency. Typically, the average absolute error in a period measurement is one or two clock cycles. This results in a relative error of 0.5 to 0.125% when the processor is operated at 8 to 16 cycles per burst. The relative error should decrease as the cycles per burst increases as a result of the absolute error remaining constant as the total number of clock cycles increases. Velocity and standard deviation measurements at 10 MHz show this trend. However, the 5 MHz data showed random changes in error with respect to cycles per burst. It also contained period measurements with absolute errors as high as 8 clock cycles. The reason for this is not known.

Several typical histograms from measurements made using the pin hole and glass fiber are shown in Figures 12, 13, 14, and 15. These histograms do not contain the single large bar and two smaller bars which the signal generator data produced. Instead, the histograms

Table 2. 5 MHz signal generator data.

CYCLES/BURST	2	4	8	16	32
Actual Clock Cycles (2ns)	200	400	800	1600	3200
Measured Clock Cycles (2ns)	201	400	799	1596	3192
Measured Frequency (MHz)	4.968	5.00	5.008	5.011	5.013
Measured Velocity (m/s)	-.139	0.0	0.033	0.048	0.056
RMS Velocity (m/s)	0.097	0.0	0.020	0.012	0.025

Table 3. 10 MHz signal generator data

CYCLES/BURST	2	4	8	16	32
Actual Clock Cycles (2ns)	100	200	400	800	1600
Measured Clock Cycles (2ns)	101	202	401	801	1601
Measured Frequency (MHz)	9.905	9.902	9.965	9.985	9.993
Measured Velocity (m/s)	-.412	-.432	-.152	-.065	-.032
RMS Velocity (m/s)	0.378	0.127	0.077	0.046	0.023

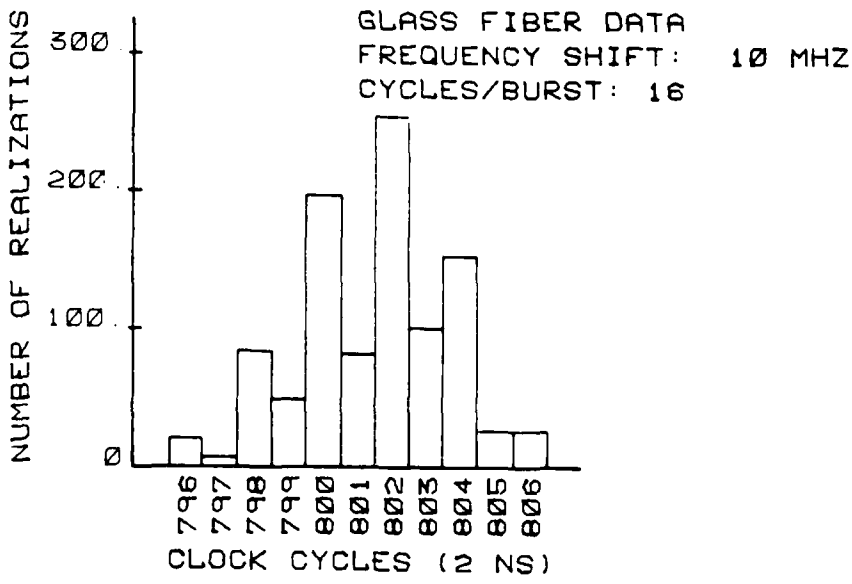

Figure 12. Histogram for 10 MHz glass fiber data.

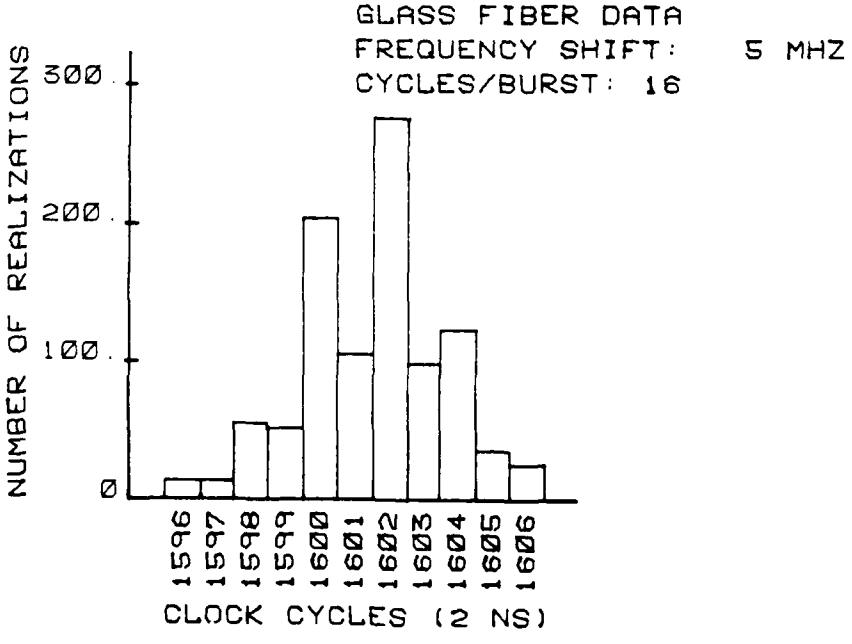

Figure 13. Histogram for 5 MHz glass fiber data.

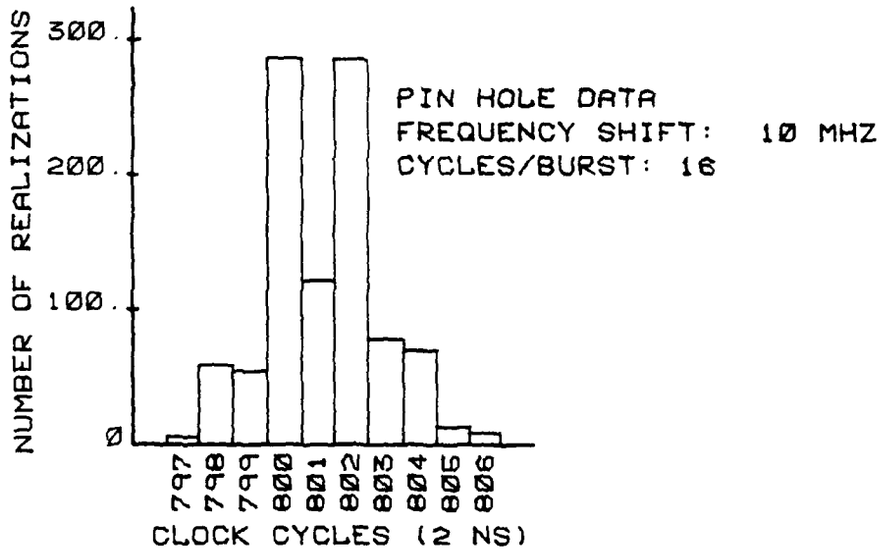

Figure 14. Histogram for 10 MHz pinhole data.

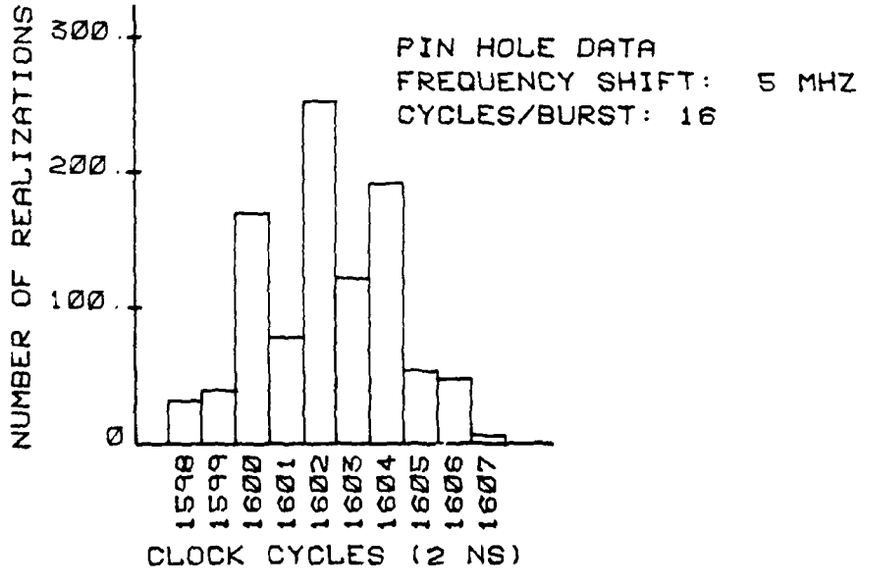

Figure 15. Histogram for 5 MHz pinhole data.

are much broader, often containing 8 or 12 bars. The spread in the histograms is probably the result of both noise in the signals and fringe distortions. The stepped nature of the histogram is thought to be the result of the processor having a perference for some digital values.

Tables 4, 5, 6, and 7 contain mean quantities calculated from the glass fiber and pinhole data. The velocity information is based on a 4.339 μm fringe spacing. (Obviously the true velocity is zero.) Once again, the average absolute clock error is one to two clock cycles with a resulting relative error of 0.5 to 0.125% for 8 or 16 cycles per burst operation. As expected, the relative error decreases as the number of cycles per burst is increased.

It should also be noted that, although the pinhole and glass fiber results are similar, the pinhole was easier to align in the probe volume and yielded higher amplitude signals.

A second TSI 1980 processor supplied by the manufacturer was checked using a signal generator in an effort to determine whether the performance of our processor was typical of this particular model. The second processor yielded histograms similar to Figure 8 for both 5 and 10 MHz signals, regardless of the cycles per burst setting. Thus, the second processor did not appear to suffer from the intermittent noise problems of the original processor nor does it have a preference for certain digital values. However, the mean quantities shown in Table 8 and 9 indicate that the second processor consistently made a measurement error of two clock cycles too many. The measurement error of the original processor varied but was often within one

Table 4. 5 MHz glass fiber data.

CYCLES/BURST	2	4	8	16	32
Actual Clock Cycles (2ns)	200	400	800	1600	3200
Measured Clock Cycles (2ns)	201	401	801	1602	3202
Measured Frequency (MHz)	4.971	4.984	4.992	4.995	4.997
Measured Velocity (m/s)	-.131	-.068	-.034	-.020	-.012
RMS Velocity (m/s)	0.362	0.158	0.080	0.028	0.019

Table 5. 10 MHz glass fiber data.

CYCLES/BURST	2	4	8	16	32
Actual Clock Cycles (2 ns)	100	200	400	800	1600
Measured Clock Cycles (2 ns)	101	201	401	802	1602
Measured Frequency (MHz)	9.902	9.943	9.967	9.981	9.986
Measured Velocity (m/s)	-.440	-.256	-.143	-.082	-.049
RMS Velocity (m/s)	0.963	0.497	0.269	0.121	0.073

Table 6. 5 MHz pinhole data.

CYCLES/BURST	2	4	8	16	32
Actual Clock Cycles (2ns)	200	400	800	1600	3200
Measured Clock Cycles (2ns)	202	402	802	1602	3203
Meausred Frequency (MHz)	4.954	4.975	4.998	4.993	4.996
Measured Velocity (m/s)	-.200	-.112	-.054	-.030	-.016
RMS Velocity (m/s)	0.203	0.105	0.054	0.027	0.013

Table 7. 10 MHz pinhole data.

CYCLES/BURST	2	4	8	16	32
Actual Clock Cycles (2ns)	100	200	400	800	1600
Measured Clock Cycles (2ns)	101	201	401	801	1602
Measured Frequency (MHz)	9.908	9.956	9.976	9.986	9.989
Measured Velocity (m/s)	-.0399	-.191	-.104	-.059	-.046
RMS Velocity (m/s)	0.637	0.355	0.178	0.093	0.035

Table 8. 5 MHz signal generator data from new processor

CYCLES/BURST	2	4	8	16	32
Actual Clock Cycles (2ns)	200	400	800	1600	3200
Measured Clock Cycles (2ns)	202	402	802	1602	3202
Measured Frequency (MHz)	4.954	4.976	4.988	4.994	4.997
Measured Velocity (m/s)	-.201	-.105	-.053	-.027	-.012
RMS Velocity (m/s)	0.065	0.033	0.016	0.008	0.004

Table 9. 10 MHz signal generator data from new processor.

CYCLES/BURST	2	4	8	16	32
Actual Clock Cycles (2ns)	100	200	400	800	1600
Measured Clock Cycles (2ns)	102	202	402	802	1602
Measured Frequency (MHz)	9.822	9.910	9.954	9.977	9.988
Measured Velocity (m/s)	-.773	-.391	-.200	-.102	-.051
RMS Velocity (m/s)	0.236	0.118	0.060	0.030	0.016

clock cycle. Thus, it is difficult to determine which, if either, processor was operating properly at all times.

It is interesting to note that in all but three of the 40 data sets the average period error was positive (too many clock cycles). According to the processor specifications, the clock error is plus or minus one clock cycle (2 ns). If this is the case the average clock error for a large number of samples should approach zero. The data presented above indicates that the probability of a positive error is greater than the probability of a negative error. Although this information is disturbing, it should be noted that at the higher cycles per burst settings one typically measures periods in excess of 1000 clock cycles. Thus, the error for 2 clock cycles is less than 0.2% of the total period.

SECTION V

EXPERIMENTAL MEASUREMENTS

1. Methodology

An ensemble average will approximate a time average if the samples are taken at equal or nearly equal increments of time. It is possible to obtain a close approximation to sampling at equal increments of time by paying careful attention to the data and sample rates. (The data rate is defined as the number of velocity signals validated per second by the signal processor.) Consider the case where the data rate is 20,000 particles per second and the microcomputer speed is at 2000 samples per second. Thus, the sampling speed is controlled by the computer which is the slower of the two devices. When the computer is ready for a sample, the TSI processor will have a point ready in a very short time due to the high data rate. As a result, the computer will be sampling at very close to 2000 points per second at nearly equal time intervals. Conversely, if the microcomputer is operating at 2000 samples per second and the data rate is 200 particles per second, the TSI processor controls the sample rate. The microcomputer will sample nearly very point the TSI processor computes and the increment between samples will depend on the arrival time between particles.

Verification that the velocity is being sampled at equal time intervals is possible by monitoring the data ready pulses produced by the processor. As described in Section III, the microcomputer samples the data at a preset time interval following the data ready pulse.

The data ready pulse can only be produced when the microcomputer is not inhibiting the TSI processor and the processor has a validated point ready. Thus, the data ready pulses occur essentially at the times when the velocity has been sampled. (There is a lag of about 3 μsec before a data ready pulse is produced following N Doppler cycles.) Oscilloscope photographs of the data ready pulse are shown in Figures 16 and 18. All photos were made with the TSI processor operating at 16 cycles per burst. The LDV had a 4.339 μm fringe spacing and a 10 MHz frequency shift. The mean flow velocity was approximately 17 m/s with a turbulence intensity of about 25%.

Figure 16a shows the data ready pulses for a data rate of 25,000 points per second. The microcomputer was not operating and, as a result, the pulses reflect the actual arrival rate of the particles. Notice that the arrival rate is random with the time between particles varying from 0.16 ms to less than 0.04 ms. The histogram of the data, shown in Figure 17, indicates the velocity varies from about 3 to 30 m/s. As a result, the residence time of the particles in the probe volume (247 μm) varies from 0.08 to 0.008 ms. Thus, it is very likely that the more closely spaced particles are the result of more than one sample being recorded from a single particle.

Figure 16b also shows the data ready pulses at a data rate of 25,000 particles per second except that the microcomputer is sampling at approximately 4800 samples per second. The data ready pulses appear much more evenly spaced than in the previous photograph and the possibility of multiple samples from a particle has been greatly reduced. However, one would still hesitate to say that the samples

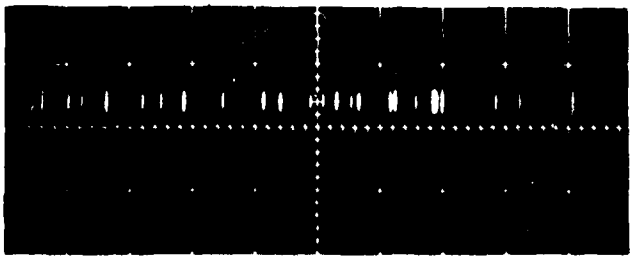

(a)

$\bar{U}$	17 m/s
Data rate	25000 s^{-1}
Sweep	0.2 ms/div
(processor free)	

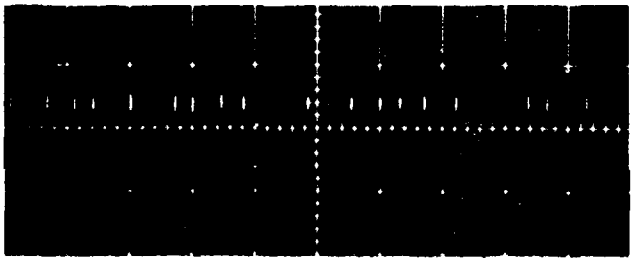

(b)

$\bar{U}$	17 m/s
Data rate	25000 s^{-1}
Sample rate	4800 s^{-1}
Sweep	0.5 ms/div

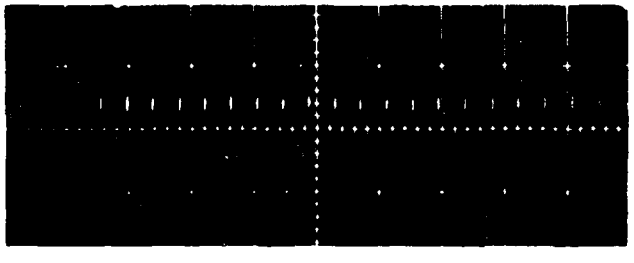

(c)

$\bar{U}$	17 m/s
Data rate	25000 s^{-1}
Sample rate	250 s^{-1}
Sweep	10. ms/div

Figure 16. Data ready pulses at a data rate of 25,000.

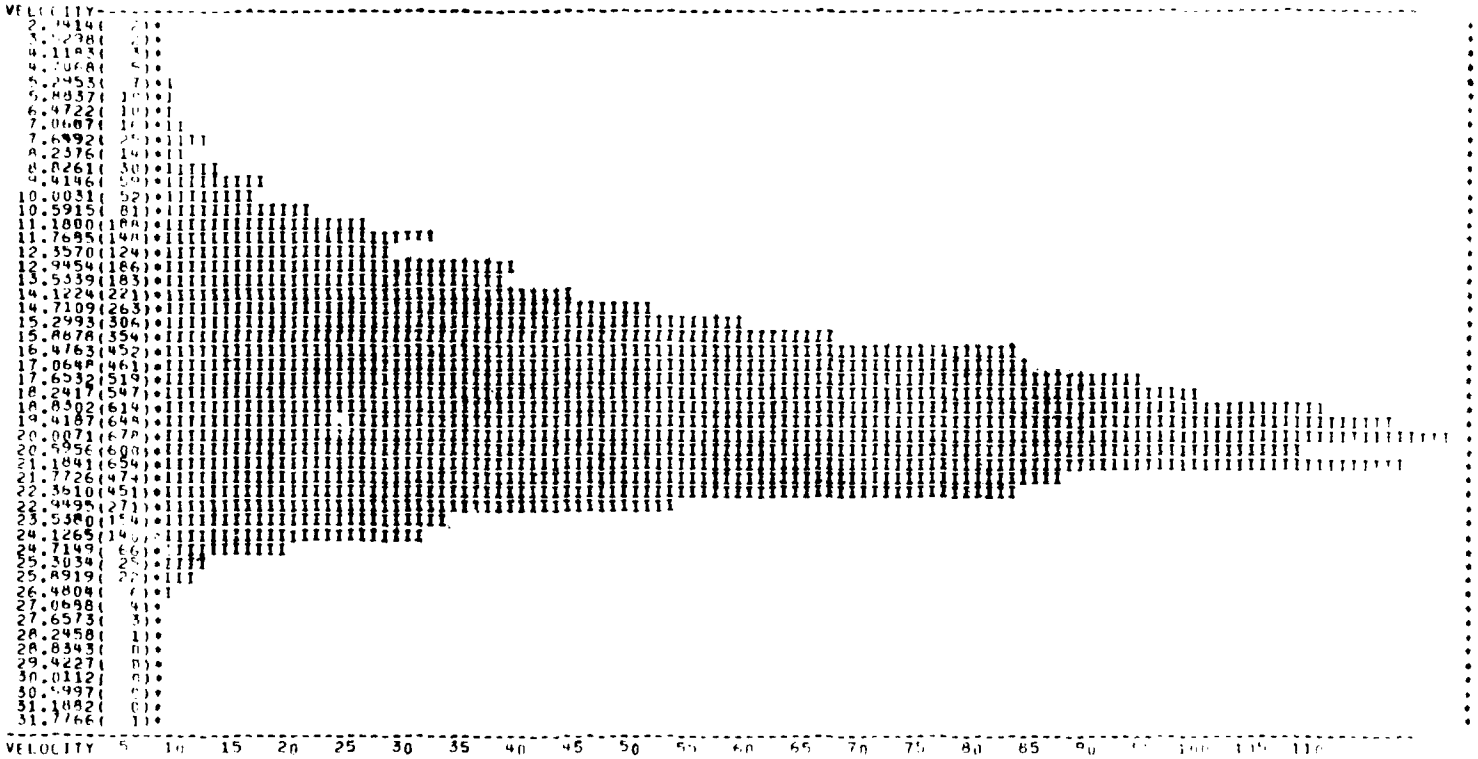

Figure 17. Typical histogram for turbulent data.

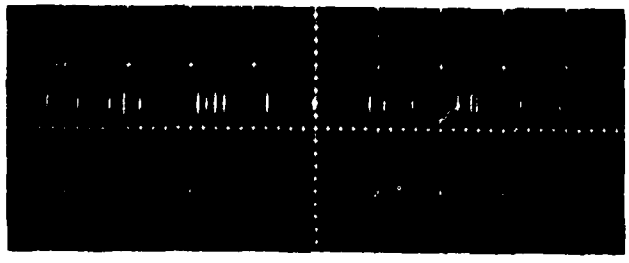

(a)

$\bar{U}$	17 m/s
Data rate	250 s^{-1}
Sweep	10. ms/div
(processor free)	

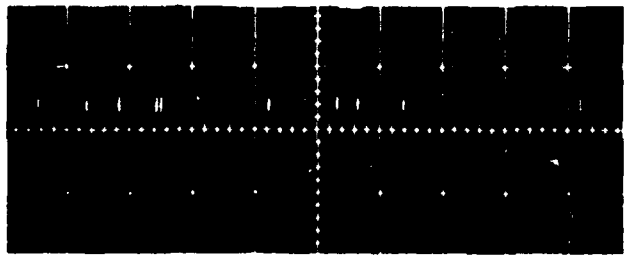

(b)

$\bar{U}$	17 m/s
Data rate	250 s^{-1}
Sample rate	4800 s^{-1}
Sweep	5. ms/div

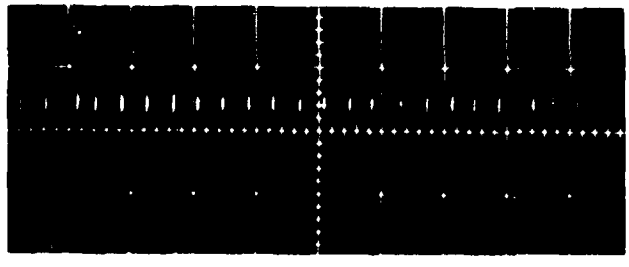

(c)

$\bar{U}$	17 m/s
Data rate	250 s^{-1}
Sample rate	25 s^{-1}
Sweep	0.1 s/div

Figure 18. Data ready pulses at a data rate of 250.

are being recorded at equal time intervals.

Figure 16c shows the data ready pulses for a data rate of 25,000 particles per second but with the microcomputer operating at 250 samples per second. At this data rate and sampling rate, the period between samples is about 100 times the average period between particle arrivals. As a result, the time between when the microcomputer is ready to take a sample and when the TSI processor has a sample ready is only about 1% of the time interval between samples. Therefore, the samples are taken at nearly equal time intervals.

In many flow systems, it is difficult to obtain data rates as high as 25,000 particles per second. Figure 18 shows data ready pulses similar to those in the previous figure except that the data rate was 250 particles per second. A data rate of 250 could easily be obtained in most flow systems. Figure 18a shows the random arrival of the particles when the microcomputer is not operating. Figure 18b shows the data ready pulses when the microcomputer sampling rate is 4800 samples per second. Because the data rate is much lower than the sample rate, the samples are recorded at a rate very nearly the same as the data rate. Thus, almost every particle that the processor validates is also sampled. However, the possiblity of multiple samples from a single particle is very small. Figure 18c shows the data ready pulses when the data rate is 250 particles per second while the sampling rate is 25 samples per second. As in Figure 16c, the samples appear to be taken at nearly equal time intervals when the sampling rate is much lower than the data rate.

Experimental measurements of velocity bias were made by looking at one point in the flow and collecting a fixed number of data points (4500 for low turbulence intensity flows, 9000 for high turbulence intensity flows) at each of several data rates. The data rate was varied by changing the seed density in the tunnel as described in Chapter III. The evaporation-condensation unit was used for all measurements to insure a nearly monodisperse aerosol of about 1 μm diameter. DOP was used as a seeding agent.

All measurements were made in one of three locations in the flow tunnel as shown in Figure 5. Low turbulence intensity (~ 1.0%) measurements were made at the center of the section just upstream of the step. Higher turbulence intensity measurements were made either at the step height and 155 mm downstream of the step (TI ≈ 20%) or 5 mm below the step and 406 mm downstream (TI ≈ 35%). All measurements were at the spanwise center of the tunnel. In all cases, the turbulence intensity is defined as the measured local RMS velocity divided by the measured local mean velocity. Both are obtained from the same data set using the uncorrected ensemble averages.

2. Experimental Data

Velocity bias is dependent on turbulence intensity. Measurements made in a low turbulence intensity or laminar flow should yield no bias. As turbulence intensity increases, velocity bias should also increase.

Figure 19 shows the measured mean axial velocity at several different seeding densitites at the low turbulence intensity point

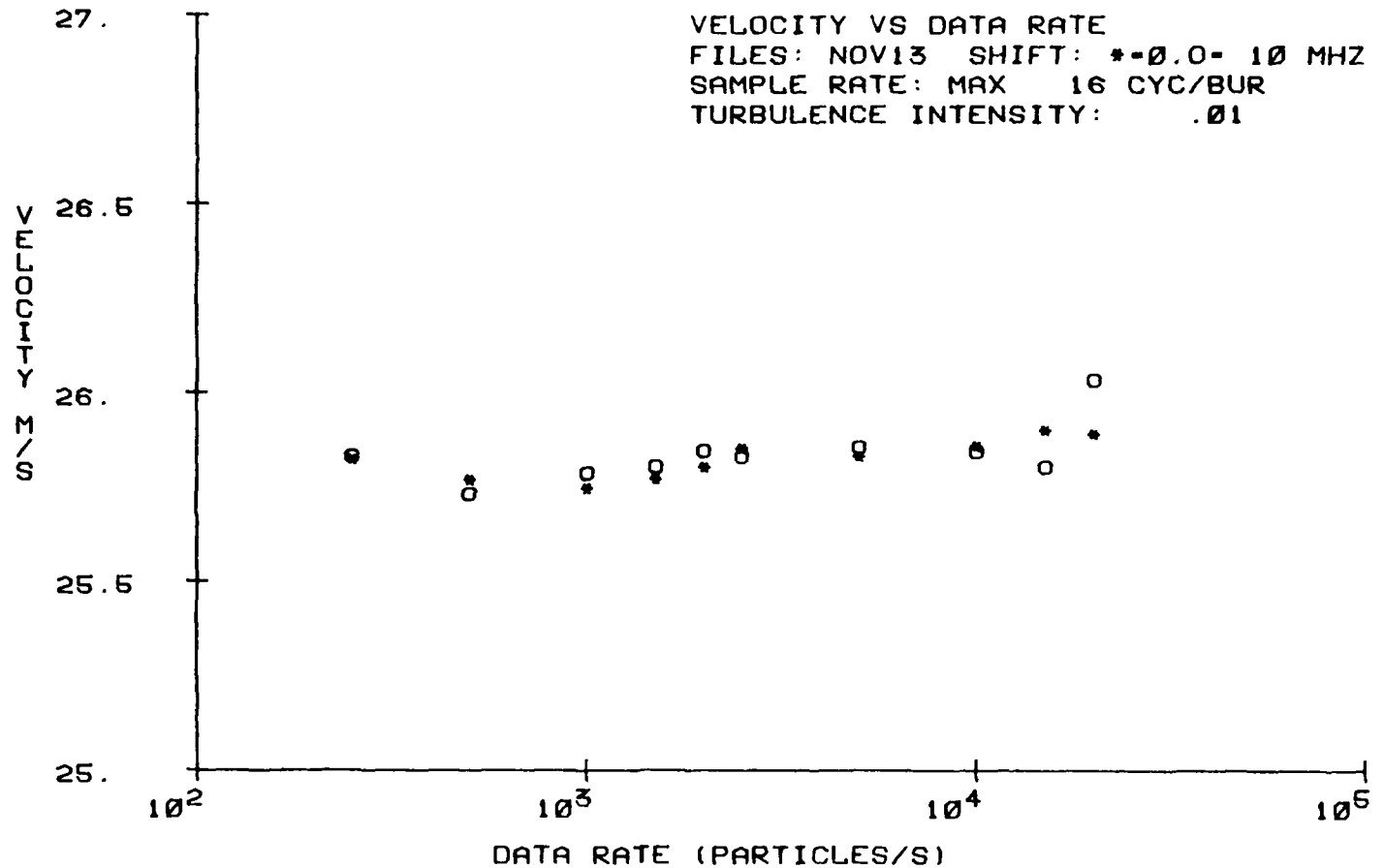

Figure 19. Velocity vs. data rate in low turbulence intensity region.

described earlier. The data were taken using frequency shifts of 0 and 10 MHz. The data rate is the rate at which the TSI processor was operating and was controlled by changing the seed density as noted above. The fringe spacing was 4.13 μm for the 0 MHz shift measurements and 4.19 μm for the 10 MHz case. Both sets of measurements were made using a 247 μm diameter probe volume and counting 16 cycles per bust. Each data point represents the mean value of about 4500 measurements. The histograms were edited using a $\pm 3\sigma$ cutoff. The maximum rate at which the microcomputer received and processed data was about 2750 samples per second. Therefore, in interpreting the measured results the data at 250 samples per second is being stored as fast as it is being processed and the resulting average velocity is an ensemble (particle) average of randomly sampled velocities. On the other hand, the data at 20,000 samples per second was being processed so fast that the computer could only sample about one point in 7. This results in an approximation to time average sampling of the data. The points at intermediate data rates are a mixture of time and ensemble averages. The figure shows that for flows with low turbulence intensity (approximately 1%) the average velocities are independent of the data rate. Thus, as expected, the ensemble average is equal to the time average.

Figure 20 is a plot of the calculated turbulence intensity corresponding to the data in Figure 19. A one percent turbulence level is about what would be expected in the flow at this point. As expected the turbulence intensity is independent of data rate in this region of the flow. The difference in turbulence intensity for the 0 and 10 MHz shifted cases is probably the result of frequency broadening due to the Bragg cells (Figures 12-15).

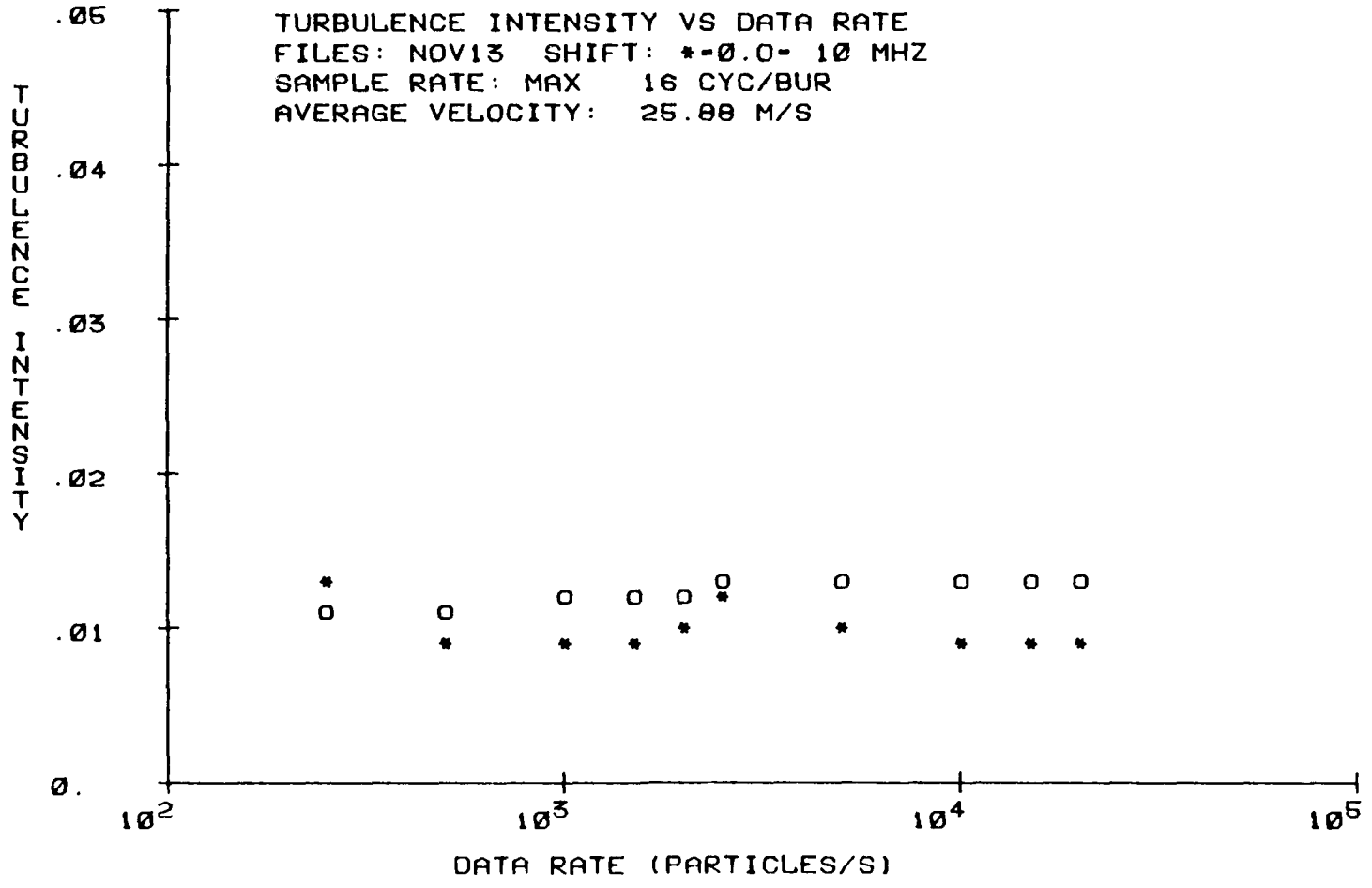

Figure 20. Turbulence intensity vs. data rate in low turbulence intensity region.

Similar measurements were made in the more turbulent region 155 mm downstream of the step with a sampling rate of 250 samples per second. Plots of the calculated mean velocity and turbulence intensity vs. data rate are shown in Figures 21 and 22. Examination of these plots reveals a trend of decreasing measured mean velocity and increasing turbulence intensity with increased data rate. In view of the earlier discussion on velocity bias, one would expect a nearly constant measured mean velocity at data rates well below the sampling rate. As the data rate approaches the sampling rate, the mean velocity based on an ensemble average should decrease. At data rates significantly higher than the sampling rate, one would again expect a nearly constant mean velocity somewhat below the initial values. Plots for turbulence intensity should have an inverted behavior. The results observed are consistent with these expectations. Figure 21 shows very little change in mean velocity at data rates from 150 to 500 particles per second. However, from a data rate of 500 to 15,000 particles per second, the mean velocity drops by about 0.875 m/s.

At data rates above 15,000 particles per second, the plot appears to be flattening out to a velocity near 18.25 m/s. If a velocity of 18.25 m/s is assumed to be the unbiased value, velocities measured at the lowest data rates contain a bias of approximately 4.8%. Velocities measured at data rates between 500 and 15,000 particles per second have varying amounts of bias, depending on the data rate.

Also included on Figure 21 are several corrected velocities calculated using the McLaughlin and Tiederman one-dimensional velocity weighting. At the lower data rates, where velocity bias is greatest,

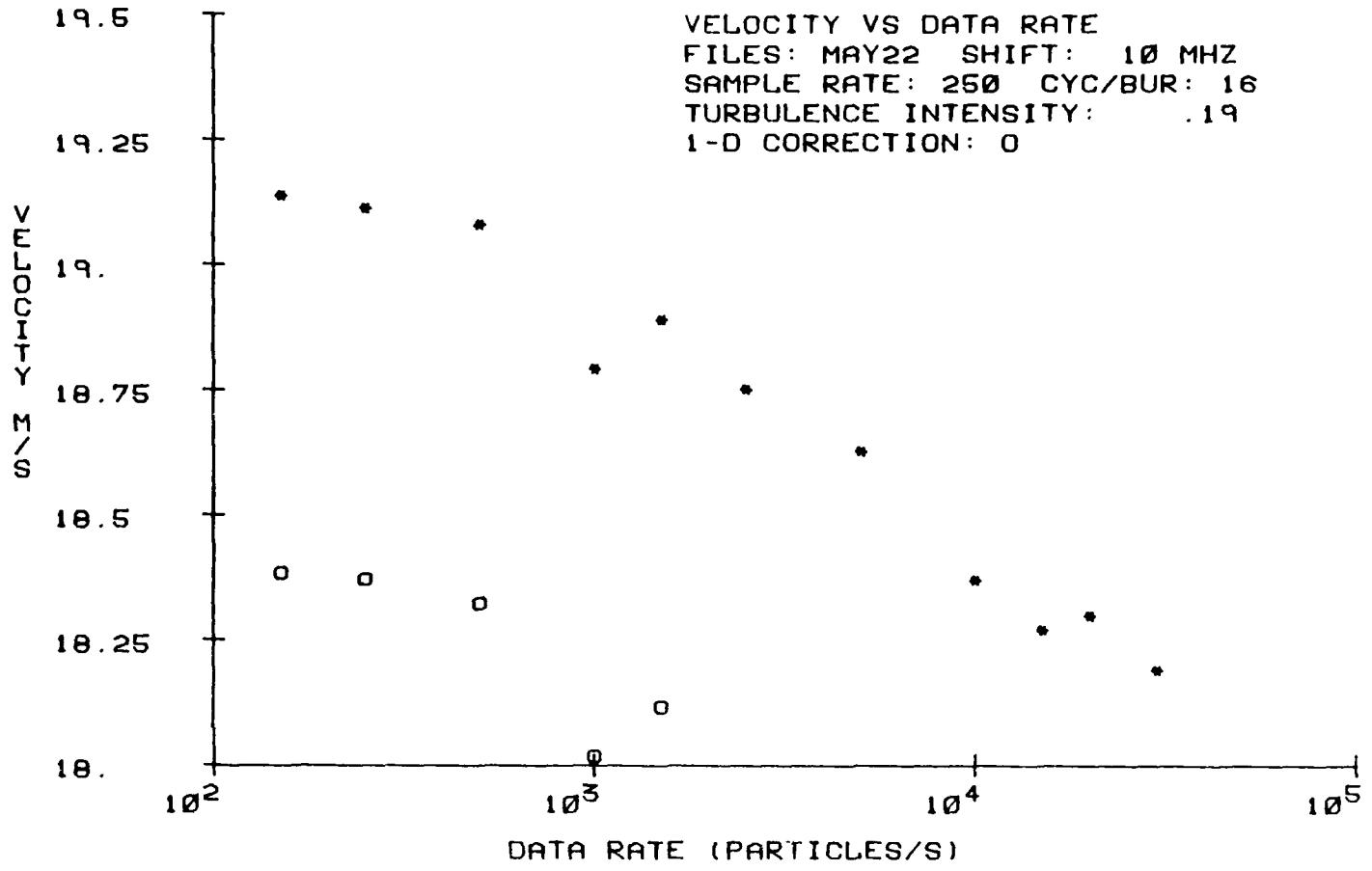

Figure 21. Velocity vs. data rate at location A.

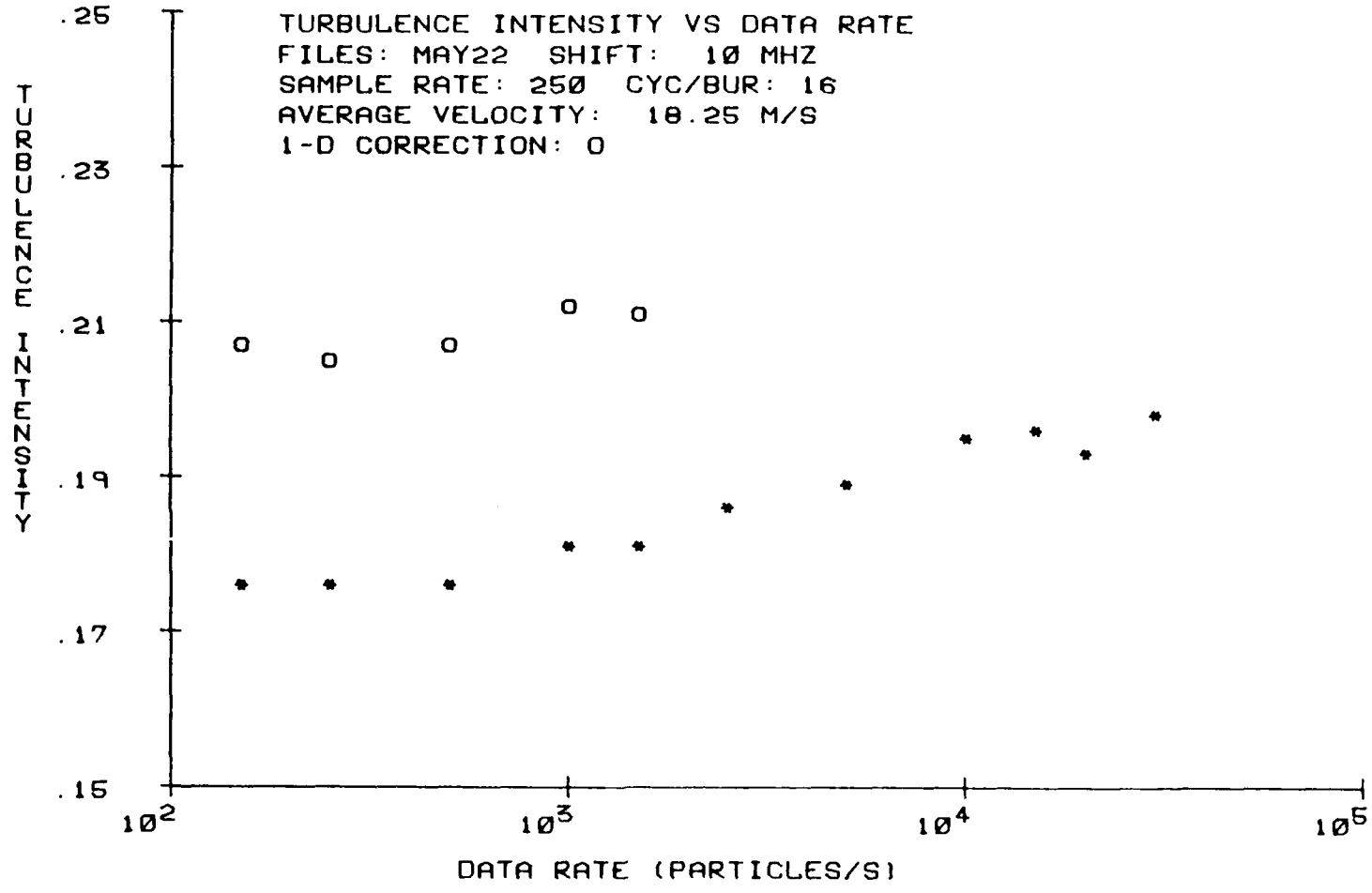

Figure 22. Turbulence intensity vs. data rate at location A.

the one-dimensional correction under corrects the mean velocity by approximately 0.7%. However, as the data rate increases, the velocity bias decreases. As a result at the higher data rates, where the velocity bias is small, the one-dimensional correction severely over corrects the data. Details of the correction scheme are in Appendix A.

Figure 22 is a plot of turbulence intensity vs. data rate corresponding to the data of Figure 21. As in the velocity plot, the measured turbulence intensity remains relatively constant at low data rates. At data rates above 500, the calculated turbulence intensity increases until the data rate reaches 15,000 particles per second. Beyond 15,000 particles per second, the turbulence intensity remains fairly constant. According to the reasoning used previously, the bias in the turbulence intensities measured at the lower data rates was approximately 10%. Figure 22 also contains several turbulence intensities calculated using the one-dimensional velocity weighting. At the lower two data rates, where the bias is greatest, the weighting over corrects by 5%. As the data rate increases, the bias decreases as before. Thus, the weighting significantly over corrects at the higher data rates.

Figures 23 and 24 are plots of velocity vs. data rate taken at the second high turbulence intensity location, 406 mm downstream of the step. Figure 23 reflects measurements at sample rates of 250 and 25 samples per second using a zero MHz frequency shift and 16 cycles/burst. Figure 24 shows velocity measurements made at the same sample rates and cycles/burst but using a 10 MHz frequency shift. Both plots show the familiar trend of decreasing mean velocity with increasing

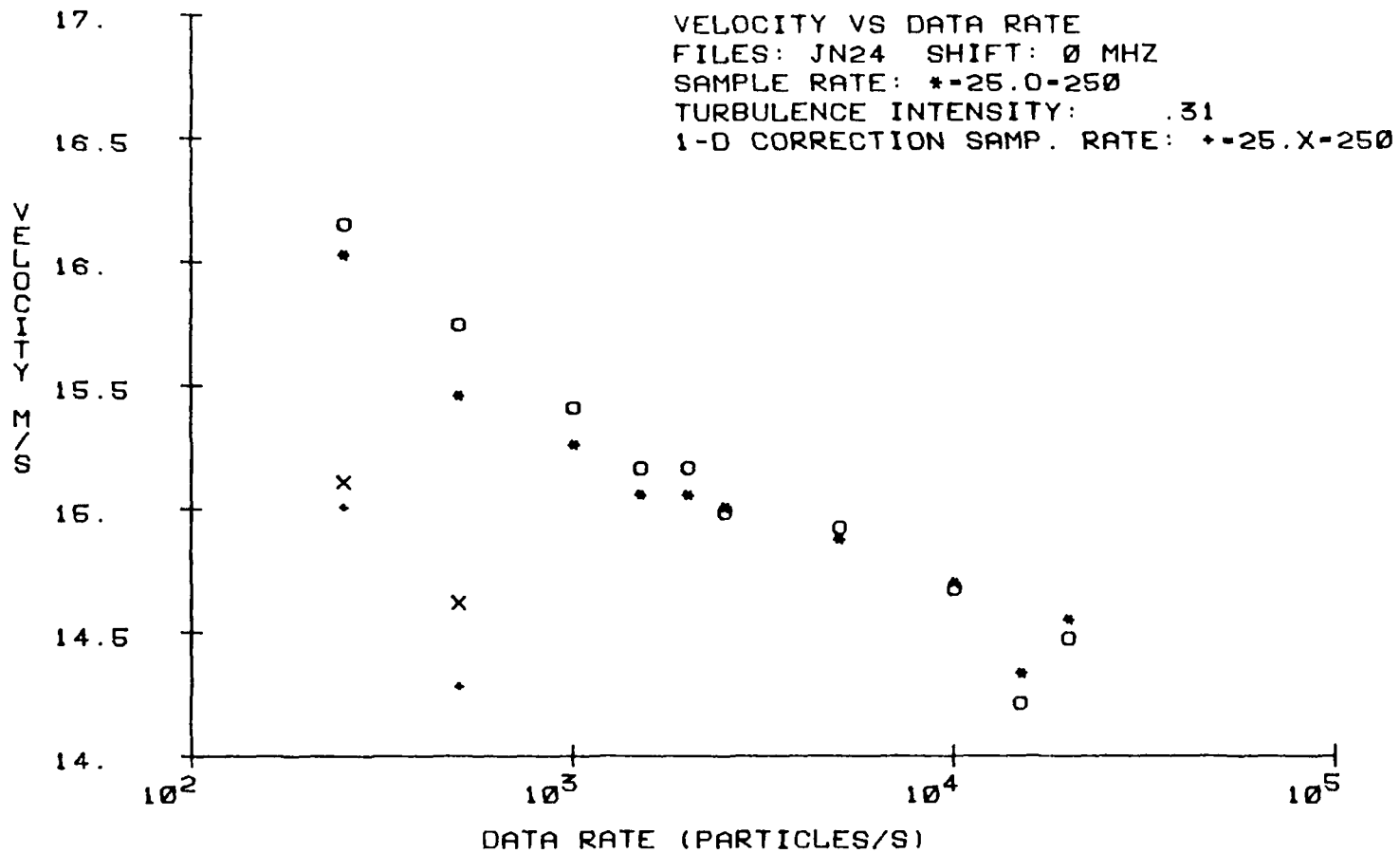

Figure 23. Velocity vs. data rate at location B (f_S=0 MHz).

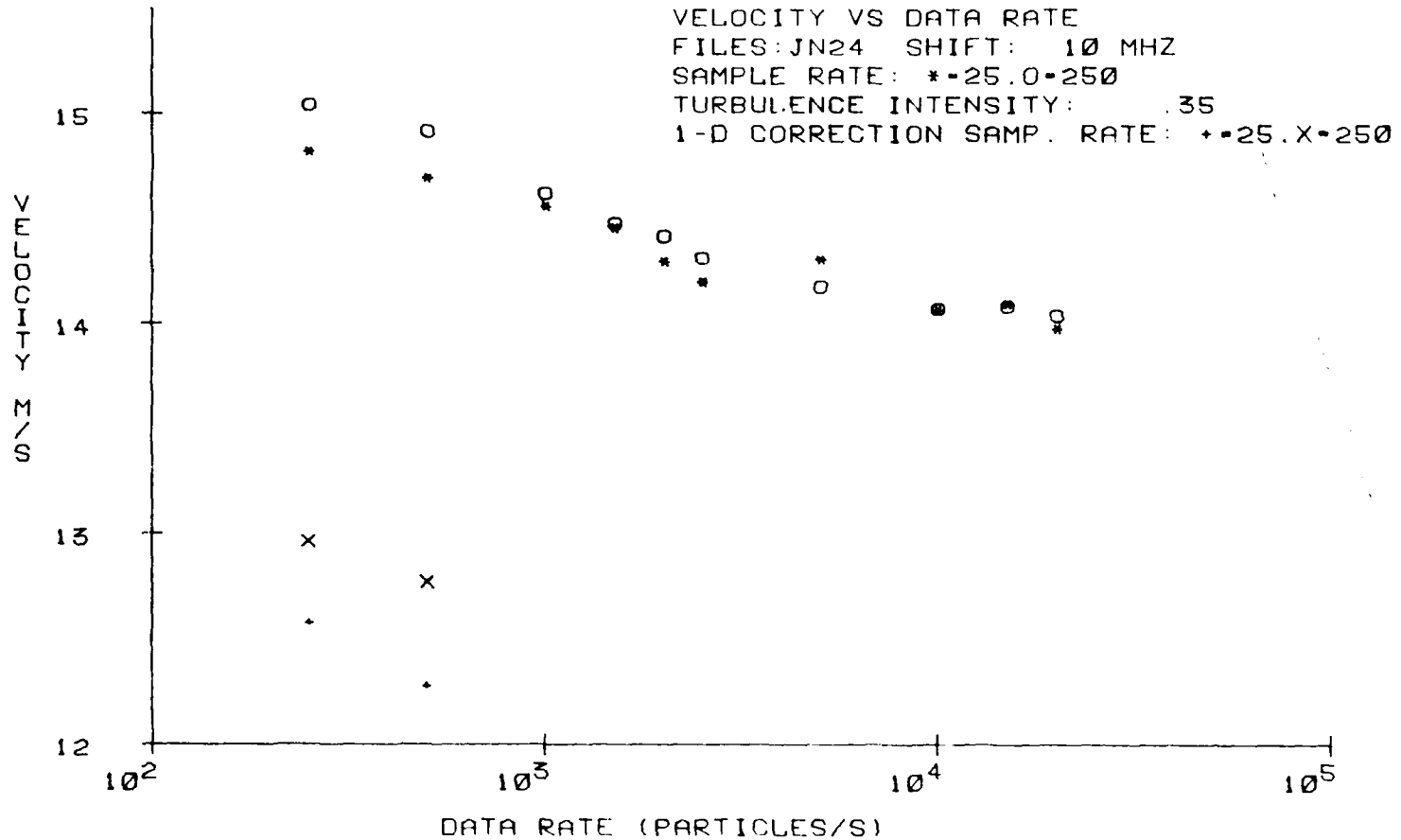

Figure 24. Velocity vs. data rate at location B (f_s = 10).

data rate and the "unbiased" mean velocity at high data rates is approximately the same whether a sample rate of 250 or 25 samples per second was used. However, the apparent bias at the lower data rates is consistently higher at the 250 samples per second sampling rate as would be expected from the previous discussion.

Figures 25 and 26 are the turbulence intensity plots corresponding to the data in Figures 23 and 24. Turbulence intensities derived from the unshifted data show a bias of about 23% at a data rate of 250 samples per second while the 10 MHz shifted data yields a bias of only 14% at the lower data rates. This difference is probably caused by incomplete signal bias. One-dimensionally corrected turbulence intensities are shown only for the unshifted data and, as before, the correction is only useful at the lowest data rates. A one-dimensional weighting seriously over corrected the 10 MHz shifted data at all data rates and, as a result, it was not included in the graph.

The possibility that incomplete signal bias existed in the unshifted data of Figure 23 is confirmed by the results shown in Table 10 which presents data taken at different N values (cycles per burst). For a frequency shift of 10 MHz the value of N had essentially no effect on the average velocity. However, at zero frequency shift the average velocity increased with N as would be expected if incomplete signal bias was present. (Increasing N reduces the effective polar acceptance angle of the probe volume and introduces a bias toward higher velocities as shown previously in Section II) A marked influence on the calculated turbulence intensity is also evident.

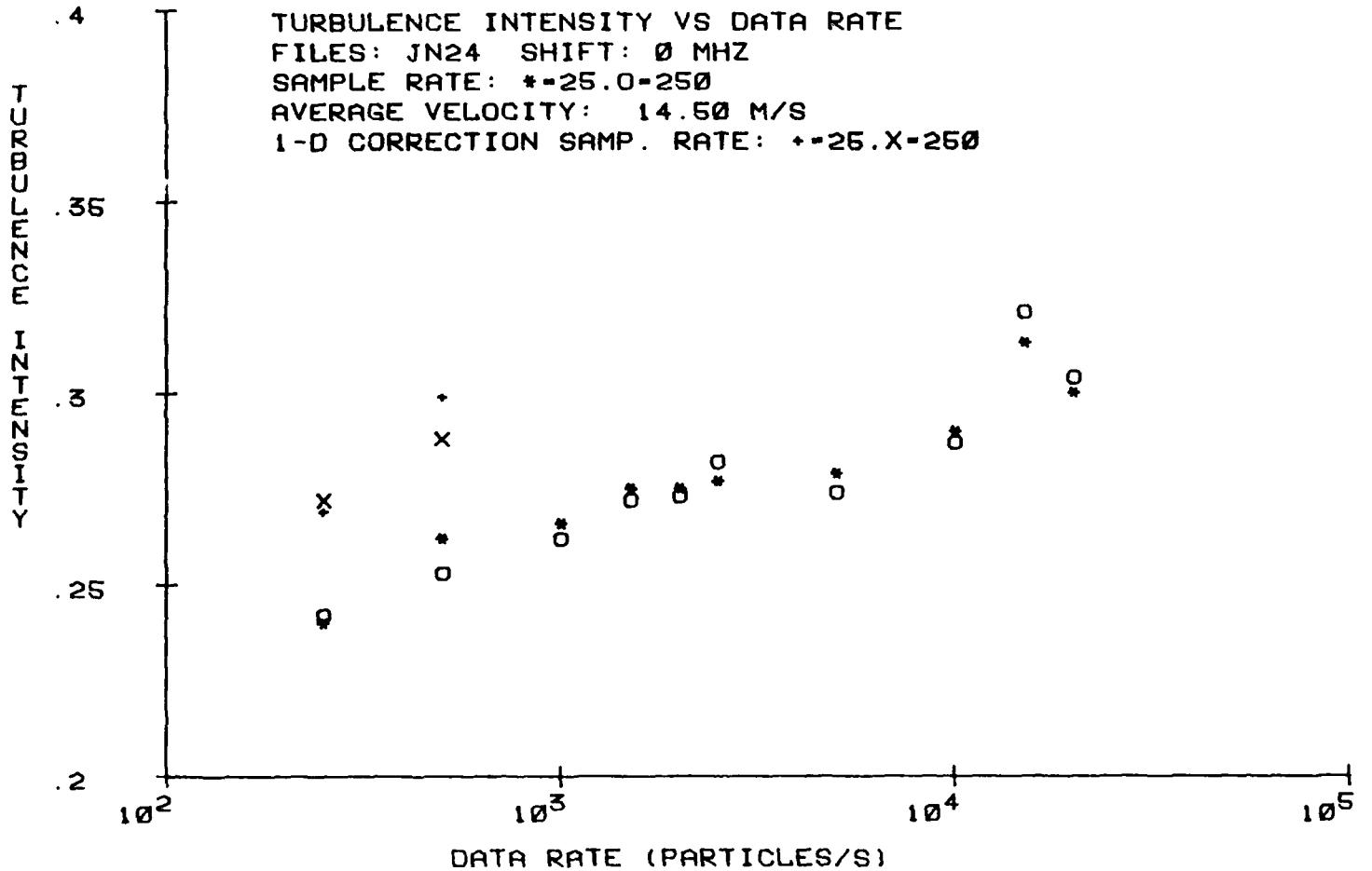

Figure 25. Turbulence intensity vs. data rate at location B (f_s=0 MHz).

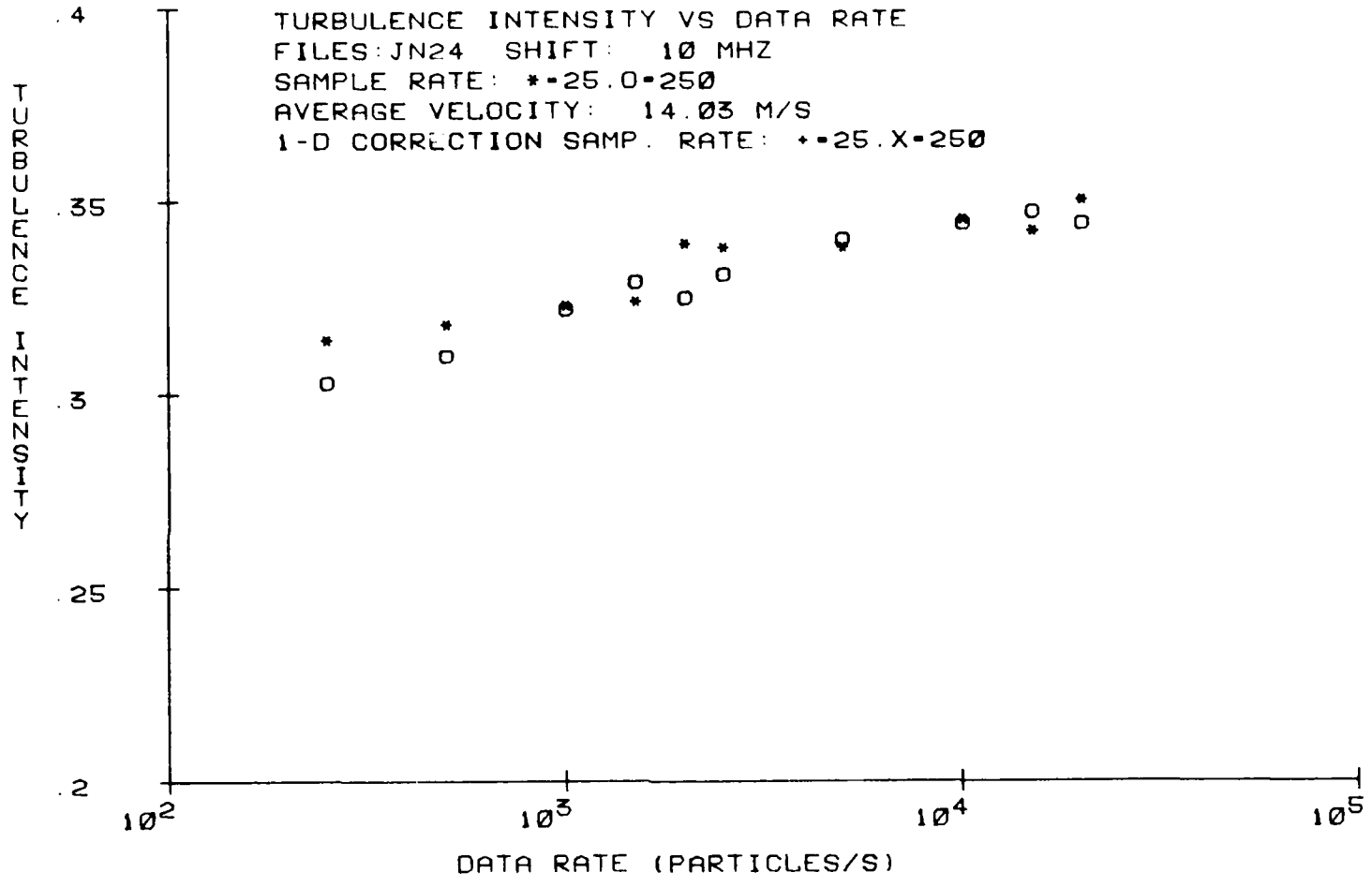

Figure 26. Turbulence intensity vs. data rate at location B (f_s=10 MHz)

Table 10. Demonstration of incomplete signal bias.

CYC/BURST	FREQ. SHIFT (MHz)	AVG. VEL. (m/s)	TURB. INTENSITY(%)[†]	SKEWNESS
8	10	14.0	34.3	-.26
16	10	14.1	34.5	-.21
32	10	14.1	34.5	-.20
8	0	14.4	30.9	+.01
16	0	14.9	27.9	+.13
32	0	15.1	25.1	+.24

[†] Turbulence intensities here, as elsewhere in this study, were calculated using the uncorrected measured mean velocity.

Table 10 also indicates the skewness of the histograms at each condition. The skewness has approximately the same negative value for all of the 10 MHz data, but is positive and increases with N for the unshifted data. Again this is consistent with the presence of incomplete signal bias. The results indicate that some incomplete signal bias existed even at the lowest value of N for the unshifted data which probably accounts for the average velocity being somewhat higher at N = 8 than that observed for the shifted data. Another possibility is that the filter used for pedestal removal cut off velocity signals near zero in the unshifted measurements. However, the 10 MHz data indicated that there were very few velocity realizations which would have been so affected. In any case this effect would have been constant with N and does not alter the conclusions relative to incomplete signal bias.

Figures 21 through 26 illustrate that both velocity bias and incomplete signal bias can be significant in turbulent flows and that a simple one-dimensional velocity bias correction is not valid at turbulence levels greater than 20 %. (It should be noted that the data shown in these figures represents a small fraction of that taken during the course of this study. All the data exhibited the same behavior.) The actual conditions under which the one-dimensional correction can be used may, of course, depend on the flow and these results should not be generalized to other situations. However, it would be useful if a general conclusion could be reached about a proper data processing method for eliminating velocity bias in measured data, since it would obviate the need for a correction.

Figures 21 through 26 suggest that it might be possible to define a ratio of data to sample rates above which a good approximation to a time average occurs, thus ensuring the absence of velocity bias. Figure 27 is a plot of the data in Figures 23 and 24 with the data rate nondimensionalized by dividing it by the sample rate. Notice that the two curves for the 10 MHz frequency shifted data (x,+) obtained at data rates of 25 and 250 samples per second converge to the same mean velocity at high nondimensionalized data rates. However, at the lower nondimensionalized data rates the two curves are divergent. The same is true for the unshifted data (*,0), although it converges to a higher mean velocity at the higher data rates due to incomplete signal bias. Thus, for example, data obtained using a data rate of 25,000 particles per second and a sample rate of 250 samples per second will yield a measured mean velocity closer to the true mean velocity than that obtained at a data rate of 2500 particles per second and a sample rate of 25 samples per second. Therefore a criterion for obtaining unbiased data based on the nondimensionalized data rate is insufficient. The actual data rate must also be above a certain value to insure unbiased data. This may have some relation to the flow structure, but further investigation is needed before any conclusion can be drawn.

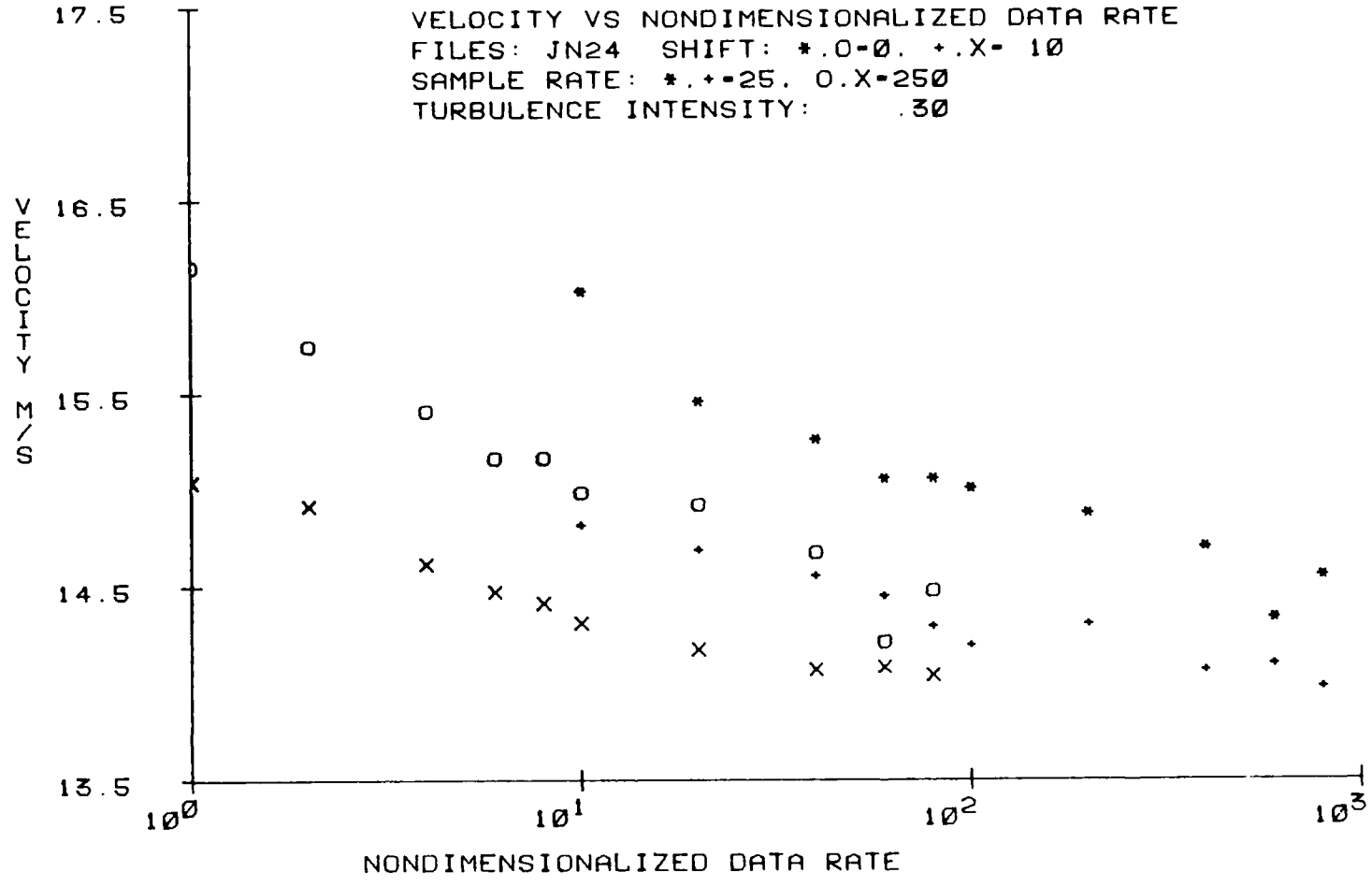

Figure 27. Velocity vs. nondimensionalized data rate.

SECTION VI

CONCLUSIONS AND RECOMMENDATIONS

Two major conclusions may be drawn from the results presented here. First, velocity bias will exist in LDV measurements made with counter type processors operating in the N-cycle mode with a magnitude related to the turbulence intensity and the data acquisition method. Second, velocity bias may be eliminated by using proper sampling techniques. The proper technique involves approximating a time average by sampling the LDV signals at a rate significantly slower than the particle arrival rate such that the data is recorded at nearly equal time intervals. However, the accuracy of the time average is apparently dependent on both the ratio of the data rate to sample rate (nondimensionalized data rate) and on the actual rate. The dependence on absolute data rate suggests that the required seeding density is related to the turbulence structure in the flow. In the present study, a good approximation to a time average was obtained when the nondimensionalized data rate exceeded 100 and the data rate was in excess of 5,000 particles per second.

Evaluation of the one-dimensional velocity weighting of McLaughlin and Tiederman showed that the accuracy of this bias correction is highly dependent on turbulence intensity and the data and sample rates used. Obviously, if the data and sample rate are such that a good approximation to a time average occurs, any correction applied to the data will actually increase the measurement error. However, for totally

biased data, the correction generally resulted in a more accurate mean velocity measurement at turbulence levels below 20 percent. Unfortunately our data processing system did not permit the effectiveness of a residence time weighting to be studied. Buchave's results [19] suggest that this weighting is more appropriate in flows with higher turbulence levels.

At the present time the only general recommendation which can be made regarding turbulent flow measurements is to vary the sampling and data rates as was done here to find the conditions at which apparently unbiased data can be obtained. This could be difficult in cases where high data rates are not attainable. Improved flow seeding may be the answer if this is the limiting factor.

Incomplete signal bias was shown to cause significant errors in turbulent flow measurements performed with an unshifted LDV. However, frequency shifting virtually eliminated the problem. The presence of incomplete signal bias is easily detected by changing the cycles per burst setting on the processor.

The results obtained in this study are based on a limited amount of data. Further work should be directed toward acquiring similar data over a wider range of data and sample rates. From this data it may be possible to develop a general criterion for obtaining unbiased measurements. However, since it appears that relatively high data rates are needed in any case, a bias correction may be necessary when high seed densities cannot be produced. Thus, further evaluation of more realistic correction schemes is needed.

LIST OF REFERENCES

[1] Hinze, J.O., Turbulence (New York: McGraw-Hill, 1975), p. 59.

[2] Proceedings from the First International Workshop on Laser Velocimetry, Stevenson, W. and Thompson, H. edtiors, Purdue University, 1972.

[3] Proceedings from the Second International Workshop on Laser Velocimetry, Stevenson, W. and Thompson, H. editors, Purdue University, 1974

[4] Proceedings of the Minnesota Symposium on Laser Anemometry, Eckert, E. editor, University of Minnesota, 1975.

[5] Laser Velocimetry and Particle Sizing, Stevenson, W. and Thompson, H. editors, Hemisphere Publishing Corp., 1979.

[6] McLaughlin, D.K. and Tiederman, W.G., "Biasing Correction for Individual Realization Laser Anemometry Measurements in Turbulent Flows," Physics of Fluids, Vol. 16, No. 12 (1973), p. 2082.

[7] George, William K., "Limitations to Measurement Accuracy Inherent in the Laser Doppler Signal," Proceedings of the LDV Symposium Copenhagen, Technical University of Denmark, 1975, p. 20.

[8] Buchave, P., "Biasing Errors in Individual Particle Measurements with the LDA - Counter Signal Processor," Proceedings of the LDV Symposium Copenhagen, Technical University of Denmark, 1975, p. 258.

[9] Barnett, D. and Bentley, H., "Statistical Bias of Individual Realization Laser Velocimeters," Proceedings of the Second International Workshop on Laser Velocimetry, Purdue University, 1974, p. 428.

[10] Hoesel, W. and Rodi, W., "New Biasing Elimination Method for Laser Doppler Velocimeter Counter Processing," Review of Scientific Instruments, Vol 48, No. 7 (1977), p. 910.

[11] Kreid, Dennis K., "Laser-Doppler Velocimeter Measurements in Nonuniform Flow: Error Estimates," Applied Optics, Vol. 13, No. 8 (1974), p. 1872.

[12] Karpuk, Michael E. and Tiederman, William G., "Effect of Finite Size Probe Volume upon Laser Doppler Anemometer Measurements," AIAA Journal, Vol. 14, No. 8 (1976), p. 1099.

[13] Eckelmann, H. and Reichardt, H., "An Experimental Investigation in a Turbulent Channel Flow with a Thick Viscous Sublayer," Proceedings of the Symposium on Turbulence in Liquids, University of Missouri - Rolla, 1971, p. 144.

[14] Meyers, James F. and Clemmons, James I., "Processing Laser Velocimeter High-Speed Burst Counter Data," Laser Velocimetry and Particle Sizing, Hemisphere Publishing Corp., 1979, p. 300.

[15] Durao, D.F.G. and Whitelaw, J.H., "The Influence of Sampling Procedures on Velocity Bias in Turbulent Flows," Proceedings of the LDV Symposium Copenhagen, Technical University of Denmark, 1975, p. 138.

[16] Durao, D.F.G. and Whitelaw, J.H., "Bias Effects in Laser Doppler Anemometry," Journal of Physics E, Vol. 13, 1980, p. 442.

[17] Giel, T.V. and Barnett, D.O., "Analytical and Experimental Study of Statistical Bias in Laser Velocimetry," Laser Velocimetry and Particle Sizing, Hemisphere Publishing Corp., 1979, p. 86.

[18] Bogard, David G. and Tiederman, W.G., "Experimental Evaluation of Sampling Bias in Naturally Seeded Flows," Laser Velocimetry and Particle Sizing, Hemisphere Publishing Corp., 1979, p. 160.

[19] Buchave, Preben, "The Measurement of Turbulence with the Burst-Type Laser Doppler Anemometer-Errors and Correction Methods," Turbulence Research Laboratory, State University of New York at Buffalo, 1979.

[20] Whiffen, M.C., Lau, J.C., and Smith, D.M., "Design of LDV Experiments for Turbulent Measurements, Laser Velocimetry and Particle Sizing, Hemisphere Publishing Corp., 1979, p. 197.

[21] Thompson, H. and Flack, R., "An Application of Laser Velocimetry to the Interpretation of Turbulent Structure," Proceedings of the ISL/AGARD Workshop on Laser Anemomety, German-French Research Institute, St-Louis, France, 1976, p. 189.

[22] Hanson, Steen, "Broadening of the Measured Frequency Spectrum in a Differential Laser Anemometer due to Interference Plane Gradients," Journal of Physics D, Vol. 6 (1973), p. 164.

[23] Durst, F. and Stevenson, W.H., "Influence of Gaussian Beam Properties on Laser Doppler Signals," Applied Optics, Vol. 18, No. 4, (1979), p. 516.

[24] Durst, F. and Zare, M., "Removal of Pedestals and Directional Ambiguity of Optical Anemometry Signals," Applied Optics, Vol. 13, No. 11 (1974), p. 2562.

[25] Wang, J.C.F., "Measurement Accuracy of Flow Velocity Via a Digital Frequency-Counter Laser Velocimeter Processor," Proceedings of the LDV Symposium Copenhagen, Technical University of Denmark, 1975, p. 150.

[26] Asalor, J.O. and Whitelaw, J.H., "The Influence of Combustion Induced Particle Variations in Laser-Doppler Anemometry," Proceedings of the LDV Symposium Copenhagen, Technical University of Denmark, 1975, p. 115.

[27] McVey, Ray, The Design of a Laser Doppler Velocimeter for use in Studying Turbulent and Mixing Flows, Master's Thesis, Purdue University, 1979.

[28] Suzaki, Yasuzi and Tachibana, Atsushi, "Measurements of μm Sized Radius of Gaussian Laser Beams Using the Scanning Knife-Edge," Applied Optics, Vol. 14, No. 12 (1975), p. 2809.

[29] Weicher, H. and Pedrotti, L.S., "A Summary of Useful Laser Equations an LIA Report," Air Force Institute of Technology, Wright-Patterson AFB.

APPENDIX

DATA ANALYSIS PROGRAM

All data analysis is performed by a FORTRAN program on the Purdue University Computing Center's CDC 6500 computer. The program consists of a main routine and four subroutines.

The main routine reads the data from disk and converts the digital information to a Doppler frequency by Equation (8) given in Section III. The Doppler frequency is used to calculate a particle velocity by

$$V_i = [\text{sgn}(f_D) - f_s\ ]f_r \qquad \text{(A-1)}$$

where V_i is the particle velocity, f_D is the Doppler frequency, f_s is the shift frequency (negative for fringes moving in the same direction as the flow), f_r is the fringe spacing, and where sgn is positive for a positive frequency shift and negative for a negative frequency shift. Once the velocities of all the data points have been determined, the main routine calls subroutine STATS to perform the statistical manipulations.

STATS determines the particle mean velocity, $\bar{U}$, the variance, $(u')^2$, the standard deviation, u', the standard deviation from the mean, σ_m, and the skewness coefficient, s, as given in the following standard equations:

$$U = \frac{1}{M} \sum_{i=1}^{M} U_i \tag{A-2}$$

$$(u')^2 = \frac{1}{M} \sum_{i=1}^{M} (U_i - \bar{U})^2 \tag{A-3}$$

$$u' = \sqrt{(u')^2} \tag{A-4}$$

$$\sigma_m = \frac{u'}{\sqrt{M}} \tag{A-5}$$

$$s = \frac{\frac{1}{M} \sum_{i=1}^{M} (U_i - \bar{U})^3}{(u')^3} \tag{A-6}$$

STATS also calculates mean velocities and standard deviations using McLaughlin and Tiederman's one dimensional velocity weighting correction scheme. However, the one-dimensional weighting produces serious errors at velocities near zero ($1/U_i = \infty$). This problem was eliminated by using a ensemble average for velocities between -.1 and .1 m/s and the weighted average for the remaining velocities. The two means were then weighted by the number of realizations in each and averaged to determine the corrected mean velocity.

A histogram of the data is plotted using subroutines HIST and USHV1. The program also contains a data editing subroutine called SELECT. SELECT edits the data set by one of three methods. The first method removes any data points which do not lie within a specific number of standard deviations from the mean. The second method allows one to specify a maximum and minimum velocity for a data set. The third method creates a histogram of the data with specific number of bins.

The bins at the ends of the histogram which do not contain the desired minimum number of velocity realizations are removed. After editing, STATS, HIST, and USHV1, are called to determine statistical quantities and plot histograms of the revised data. A typical histogram of velocity data created before and after editing the data with a 3σ cutoff are shown in Figures A1 and A2. Generally, the 3σ cutoff was used to edit the data set, and it was found to work well at elminating extraneous data points.

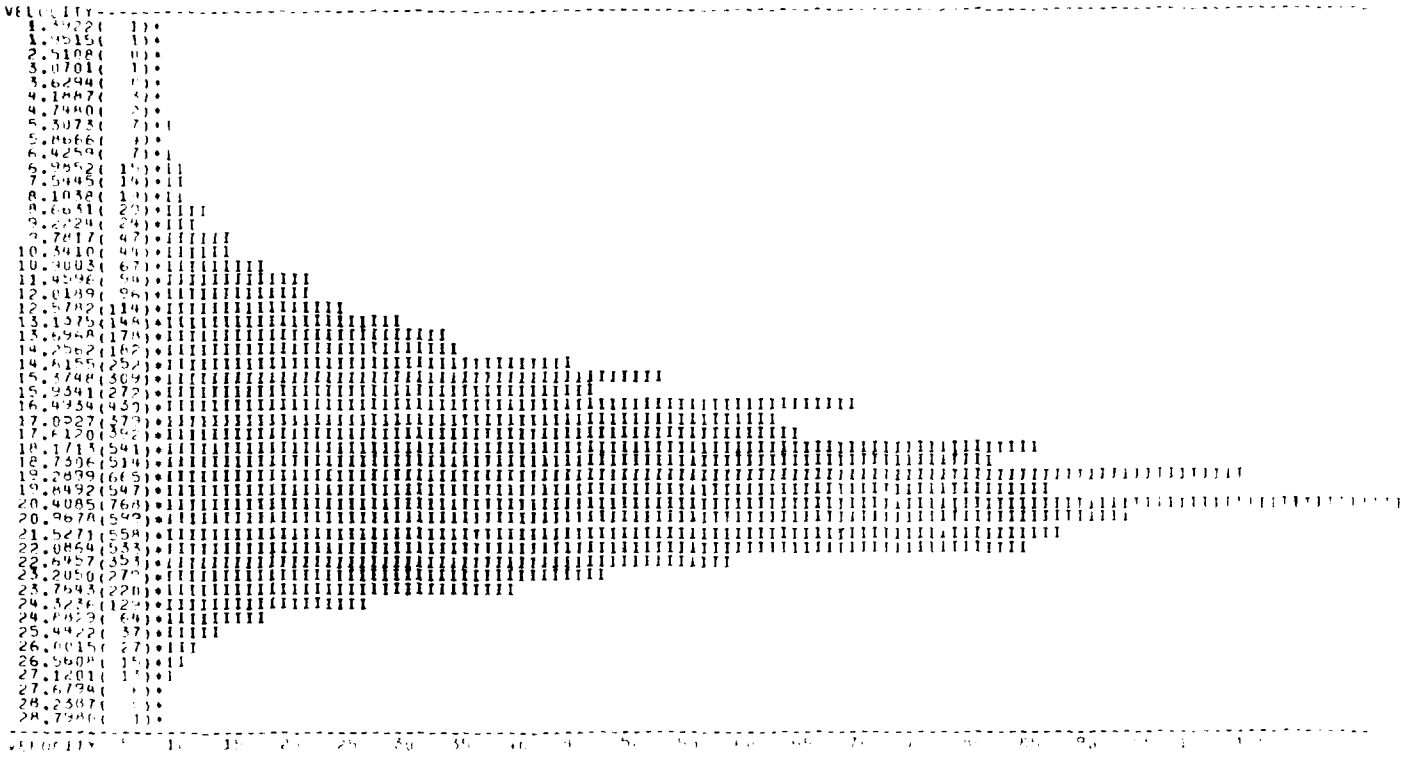

Figure A1. Typical velocity histogram before editing.

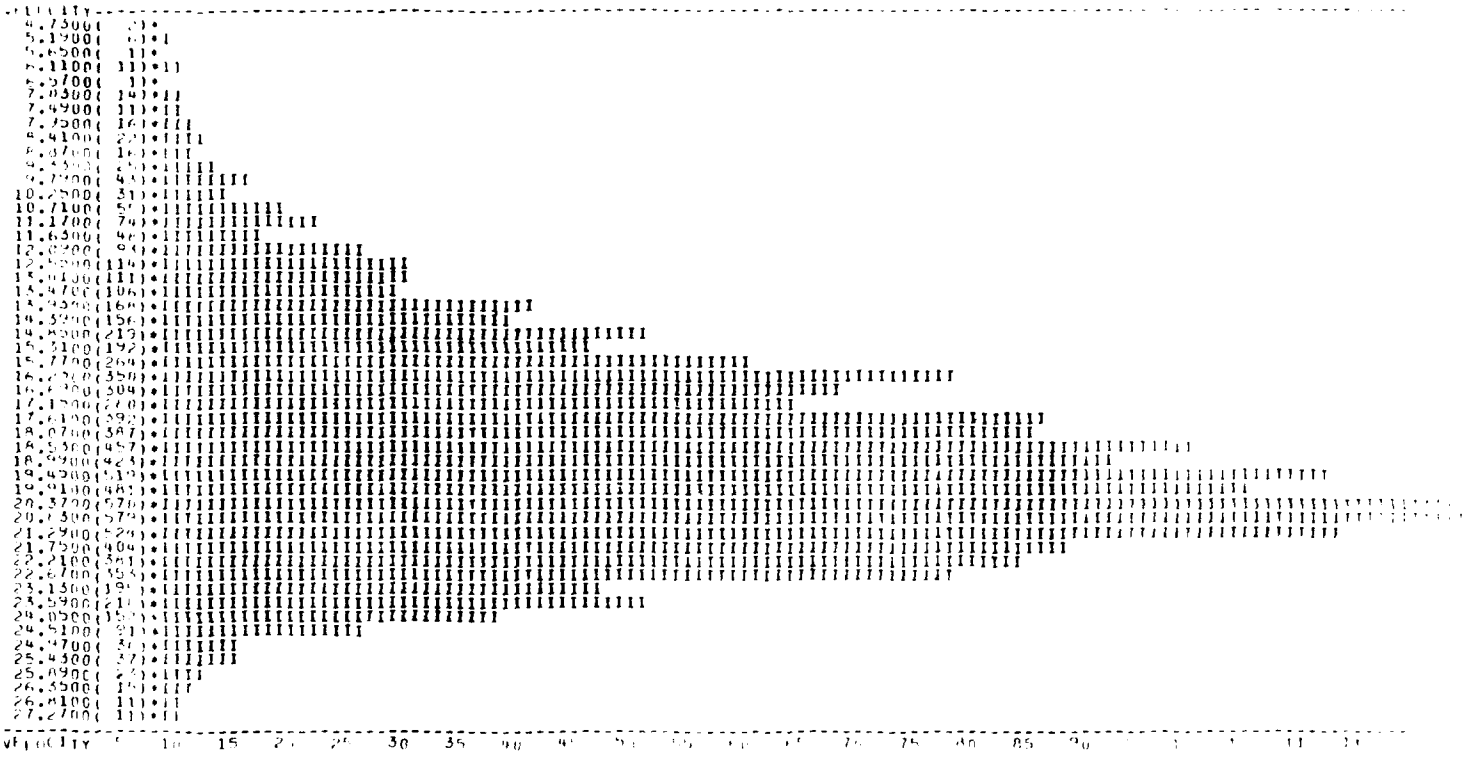

Figure A2. Typical velocity histogram after editing.

U.S.Government Printing Office: 1981 - 757-002/413

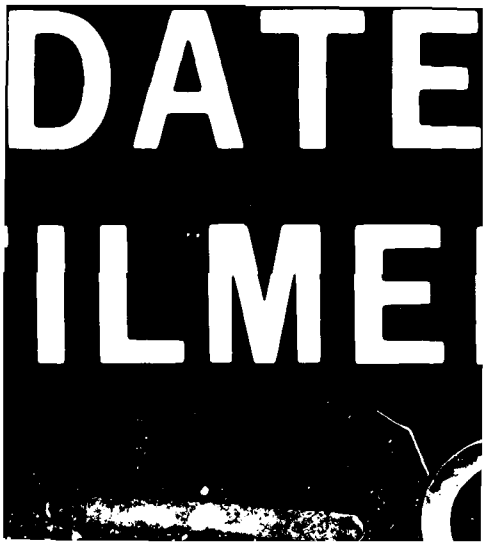
DATE
ILME